CEIS TOR VERGATA Research Papers

Università di Roma Tor Vergata

ISSN 2610-931X

CEIS Tor Vergata

RESEARCH PAPER SERIES

Vol. 19, Issue 5, No. 517 – July 2024

Identifying Economic Shocks in a Rare Disaster Environment

Luisa Corrado, Stefano Grassi and Aldo Paolillo

Identifying Economic Shocks in a Rare Disaster Environment*

Luisa Corrado† Stefano Grassi‡ Aldo Paolillo§

July 12, 2024

Abstract

We propose a new approach to efficiently estimate and analyze DSGE models subject to large shocks. The methodology is applied to study the macroeconomic effect of these unusual shocks in a new Two-Sector model with heterogenous exposure to the COVID-19 pandemic across sectors. We solve the model nonlinearly and propose a new nonlinear, non-Gaussian filter designed to handle large shocks and identify their source and time location. Monte Carlo experiments show that the estimation and identification of large shocks is feasible with a massively reduced running time. Empirical results indicate that the pandemic-induced economic downturn can be reconciled with a combination of large demand and supply shocks. Finally, we present a set of counterfactual experiments to filter out potential demand and supply shock complementarities, and perform a robustness exercise to check the sensitivity of the model parameters to large shocks.

JEL codes: C11, C51, E30.

Keywords: COVID-19, DSGE, Large shocks, Nonlinear, Non-Gaussian.

*An earlier version of this paper was published in the CEIS Research Papers Series under the title "Modelling and Estimating Large Macroeconomic Shocks During the Pandemic".

We thank seminar participants at the University of Rome "Tor Vergata", the Sichuan University, the BI Norwegian Business School, the Federal Reserve Bank of Chicago and the University of Perugia and conference participants at the ASSA 2021 Annual Meeting, the CEF 27th International Conference, the IAAE 2021 Annual Conference, the 11th RCEA Money-Macro-Finance Conference, the EEA-ESEM 2021 Congress and the Delhi Winter School 2021 Conference. Among others we thank Federico Ravenna, Ambrogio Cesa-Bianchi, Martin Bodenstein, Marco Sorge, Marco Del Negro, Andrea De Polis, Paolo Gelain and Francesco Ravazzolo for useful comments. Stefano Grassi gratefully acknowledges financial support from the University of Rome "Tor Vergata" under Grant "Beyond Borders" (CUP: E84I20000900005).

†Department of Economics and Finance, University of Rome 'Tor Vergata' and RCEA. Address: Via Columbia 2, Rome (00133), Italy. Email: luisa.corrado@uniroma2.it.

‡Department of Economics and Finance, University of Rome 'Tor Vergata' and CREATES. Address: Via Columbia 2, Rome (00133), Italy. Email: stefano.grassi@uniroma2.it.

§Department of Economics and Finance, University of Rome 'Tor Vergata'. Address: Via Columbia 2, Rome (00133), Italy. Email: aldo.paolillo@uniroma2.it.

1 Introduction

Modern economies are increasingly exposed to shocks of large magnitude that pose new research challenges in the specification and estimation of macroeconomic models. The presence of large unprecedented shocks is particularly evident in the case of the COVID-19 pandemic in 2020. The drastic measures taken have resulted in a sudden global economic disruption, leading to one of the worst recessions since the Great Depression. The macroeconomic effects are unprecedented in nature and magnitude and require the development of new economic models and methods, see Lenza and Primiceri (2022).

From a macroeconomic point of view, the COVID-19 pandemic raises questions about its possible classification as a supply shock or demand shock, since production and consumption are affected. Safety concerns hamper the production and consumption of goods in contact-intensive sectors, leading to cascading effects on other sectors that increase economic losses.

This paper contributes to the emerging literature on the economic effects of the pandemic by bridging a structural macroeconomic model with the data. In this respect, a key contribution is to build and estimate a medium-scale New Keynesian dynamic stochastic general equilibrium (NK-DSGE) model that features large shocks alongside nominal frictions in prices and wages, real frictions on investment, variable capital utilization, habits in consumption, and a zero-lower bound (ZLB) on the nominal interest rate.

The model is estimated using US time series, which include the COVID-19 periods. As the economic impact of social distancing and containment policies is largely asymmetric between industries, the model includes two sectors with different degrees of exposure to the pandemic. In the data, we identify the US Leisure and Hospitality[1] as the most affected sector and the other sector as the rest of the economy (general sector).[2]

Although the leisure and hospitality sector represents only about 4% of the US economy, it contributes to a relevant share (around 2 percentage points) of the drop in GDP from the pandemic (-9%), as its production has almost halved. The leisure and hospitality industry is the sector hardest hit by abnormal shocks due to its contact-intensive

[1] According to the Bureau of Economic Analysis (BEA) and Bureau of Labor Statistics (BLS) industry classification.

[2] A recent contribution by del Rio-Chanona et al. (2020) finds that the effects of the pandemic vary greatly between different industries. Although there are no negative value-added effects for less contact-intensive industries such as legal services, power generation, and distribution, or scientific research, the expected value-added loss reaches the maximum for leisure and hospitality.

nature, with a quarterly growth rate of -40% in employment and -45% in value added during the second quarter of 2020.

To study the characteristics of the pandemic, our model considers large shocks in the demand for pandemic-sensitive products and in the demand for the general sector. In addition, we study the large-scale shocks arising from labor supply and productivity in both sectors and their joint effect on the macroeconomy. To account for the large movements in the time series during the COVID-19 outbreak, we allow demand and supply shocks to occasionally be drawn from various large shock components with inflated variability for some of them. In this environment shocks can feedback on each other: for example, as wages for work decline, there will be potentially larger second-order negative effects on demand and the possibility of a self-reinforcing downward spiral in production, employment, income and demand.

These features generate nonlinearity and non-Gaussianity in the model and, to make inference, we propose a new nonlinear, non-Gaussian filter designed to handle and identify large pandemic shocks. The key contribution of our filter is to provide an estimate of both the ex-ante and ex-post probabilities of a large shock, which are endogenously estimated together with the DSGE parameters. Moreover, the proposed filter can distinguish between cases where shocks originate from a component with only one large shock, a combination of some large shocks, or all large shocks.

The proposed inference strategy is a general methodology that may be used in time series models in which the identification of large shocks must be done in a computationally feasible way.

Our results show that the economic disruption caused by the pandemic can be explained by a combination of large demand and supply shocks. In the second quarter of 2020, the filter detects a large negative shock in the demand for all types of goods, together with a large negative shock in the demand for contact-intensive products. On the supply side, we detect a large labor supply shock in the general sector and a large labor productivity shock in the pandemic-sensitive sector.

Our paper links and contributes to three strands of the literature: the theoretical analysis of the economic effects of the Coronavirus pandemic; the empirical literature that fits time-series models with pandemic related data; and the methodological research on

the use of nonlinear, non-Gaussian filters designed to deal with large shocks.

On the theoretical side, this paper is related to the literature that studies the role of sectoral heterogeneity in the transmission of pandemic shocks. Guerrieri et al. (2020) use a stylized production economy model to assess whether a negative labor supply shock can cause a demand compression greater than the shock itself. These complementary shocks, called *Keynesian supply shocks*, can occur in a multisectoral model but not in a single sector set-up. The role of complementarities is further explored by Baqaee and Farhi (2021) in the framework of a rich input-output production network. Woodford (2020) shows that in a multi-sectoral model with incomplete financial markets, the circular flow in the network of payments can be altered as a result of supply disruptions, which are concentrated in some sectors, leading to inefficient demand even without the assumption of complementarities in preferences and technology. Our paper abstracts from complementarities in production and imperfect financial markets but examines how preferences and rigidities affect the transmission of shocks.

This paper is also connected to the literature that deals with the economic effects of the pandemic by using calibrated DSGE models. Faria-e Castro (2021) uses a two-sector DSGE model with borrowing constraints to analyze how a shock to the utility of contact-intensive services propagates to other sectors and studies the subsequent fiscal policy response. Fornaro and Wolf (2020, 2023) model the pandemic as a negative shock to total factor productivity, which can generate long-term economic losses in a New Keynesian DSGE set-up with endogenous growth. Unlike these authors, our specification of pandemic shocks (see Section 3) allows for agnostic combinations of many economic forces, thus providing a flexible decomposition of the shock into usual business cycle disturbances.

The previous papers allow only one type of pandemic-related shock, one at a time. Unlike their set-up, our model allows the pandemic to generate different types of shocks that together hit the economy and assess their relative importance. Differently from the literature that focuses on *Keynesian supply shocks*, in our study, we consider reasonable that the pandemic recession can depend both on productivity forces (production is interrupted due to the closure of industrial activities) and on demand forces (consumption is more difficult for the containment measures). Therefore, in our model preference and productivity shocks coexist, and we estimate their relative importance.

Following Abo-Zaid and Xuguang (2020), we build a New Keynesian model with two sectors affected differently by the pandemic and extend the model in different directions. First, we allow the pandemic to affect labor supply and labor productivity simultaneously. Secondly, to fit the data, we enrich the model with these additional features: capital frictions in the form of variable capital utilization; imperfect competition and wage rigidities in labor markets; habits in consumption; and a zero-lower bound on the nominal interest rate.

Another part of the literature focuses on epidemiological models see, among others, Fernández-Villaverde and Jones (2022), Eichenbaum et al. (2022, 2021), Bodenstein et al. (2020) and Kaplan et al. (2020). Instead, we consider the pandemic shocks to be exogenous, as the optimal balance between health and economic activity is outside the scope of this paper. The approach to analyzing the economic consequences of the COVID-19 pandemic without an integrated epidemiological model has also recently been explored by Ferroni et al. (2022).

On the empirical side, this paper contributes to the literature that fits time series models to pandemic data. Lenza and Primiceri (2022) estimate a Vector Autoregressive model (VAR) without discarding the extreme movements of 2020. They allow for the possibility of large shocks, consisting of a lifted standard deviation of innovations. The strategy of Lenza and Primiceri (2022) has also been recently adopted by Cardani et al. (2022), who estimate a DSGE model with pandemic shocks using data from the euro area. We differ from Lenza and Primiceri (2022) by exploiting the structural nature of our DSGE model to test the occurrence of just some combination of large shocks, rather than necessarily all of them together (similarly to what was proposed more recently in the VAR setting by Carriero et al., 2022).

Our paper is also related to the literature on fat-tailed shocks in DSGE models, such as in Cúrdia et al. (2014) and Chib and Ramamurthy (2014). Due to the severity of the recession caused by the pandemic, we use different model assumptions for economic shocks than those used for these contributions, as discussed in Section 3. From a methodological point of view, this paper is related to the filtering and estimation of DSGE models. Among others, Fernández-Villaverde and Rubio-Ramírez (2007), Fernández-Villaverde et al. (2011) and Flury and Shephard (2011) apply the Particle Filter (PF) to DSGE estimation, while

deterministic filters such as the Central Difference Kalman Filter (CDKF), the Unscented Kalman Filter (UKF), and the Quadratic Kalman Filter (QKF) have been used by Andreasen (2012a, 2013), Ivashchenko (2014), Kollmann (2015), Noh (2020) and Benigno et al. (2020).

The possibility of large shocks generates higher-order effects and interactions among variables that requires a nonlinear solution. In this case, the standard Kalman Filter (KF) cannot be applied, and nonlinear non-Gaussian filters, such as PFs, are needed to approximate the likelihood and filter out the latent states. Unfortunately, PFs become quickly computationally unfeasible due to the increasing number of state variables. Moreover, large shocks are an additional blow to the effectiveness of PFs, as they require a huge number of particles to describe all the possible outcomes that can occur after a large shock, see Pitt and Shephard (1999) and Amisano and Tristani (2011).

To solve this issue efficiently, we propose a new nonlinear, non-Gaussian filter that is based on Mixtures of Mixtures of Cubature Kalman Filter (MM-CKF). The Cubature Kalman Filter (CKF) of Arasaratnam and Haykin (2009), is a nonlinear filter that has been used successfully in engineering applications. Although similar to the UKF (Wan and Van Der Merwe, 2000) is more stable, accurate and allows for a square root solution that further improves its stability, see Arasaratnam and Haykin (2009).[3] The MM-CKF proposed in this paper runs banks of CKFs in parallel and tests the location and plausibility of each (possible) combination of large and ordinary shocks. To avoid an exponential growth in the number of filtering components, a collapse procedure is proposed to retain only the mixands with the largest weights. To our knowledge, the closest filter to ours is given in Binning and Maih (2015). They use mixtures of Gaussian filters, including the CKF, in a regime-switching DSGE model. Unlike our paper, they do not estimate the model and only run an exercise with calibrated parameters.

Extensive Monte Carlo experiments show that MM-CKF allows to estimate DSGE models with large shocks and identifies the type and time location of the shocks with a significantly reduced running time (in this large shock environment, the running time of the proposed procedure is around two orders of magnitude lower than that of competing PFs). Model parameters are estimated using the Sequential Monte Carlo (SMC) sampler

[3]Both the UKF and the CKF use a weighted set of symmetric points, but they are chosen differently. For a detailed description of the advantages of the CKF over the UKF, see Arasaratnam and Haykin (2009).

proposed by Creal (2007, 2012) and Herbst and Schorfheide (2014, 2015). This estimation strategy has great advantages in parallelization, possible multimodality detection, and online estimation, as pointed out by Herbst and Schorfheide (2014) and Cai et al. (2021). Finally, we present a set of counterfactual experiments to filter out potential demand and supply shock complementarities, and perform a robustness exercise to check the sensitivity of the model parameters to large shocks.

The remainder of the paper is organized as follows. Section 2 describes the new Two-Sector One-Agent model that features large shocks. Section 3 discusses the large shock specification and the model solution. Section 4 discusses filtering problems in the presence of large shocks. Section 6 presents the filtering algorithm and performs Monte Carlo experiments. Section 7 estimates the model on US data. Finally, Section 8 concludes. Derivations, data description, and further empirical results are reported in the Appendix.

2 Model Description

The economy consists of a representative household, wholesale and retail firms, unions, and a central bank. Figure 1 shows that the household consumes two final goods, one from the general sector and the other from the pandemic sensitive sector (Leisure and Hospitality). They also supply labor and rent capital to wholesale firms in both sectors. The wholesale firms operate the production technologies and sell the products to the retail firms, which set prices in the monopolistic competitive final goods markets. The unions act as intermediaries between the household and the wholesale firms and introduce contractual wage stickiness in both sectors. Finally, the central bank is responsible for conducting monetary policy. From now on, the general sector will be denoted as Sector 1 ($\mathcal{S}_1$), while the Leisure and Hospitality sector will be indicated as Sector 2 ($\mathcal{S}_2$).

Households

Households choose the sequence of consumption for the two goods ($c_{1,t}$ and $c_{2,t}$), the sequence of hours worked in the two sectors ($n_{1,t}$ and $n_{2,t}$), the amount of next period capital in the two sectors ($k_{1,t}$ and $k_{2,t}$), and the level of capital utilization in the production

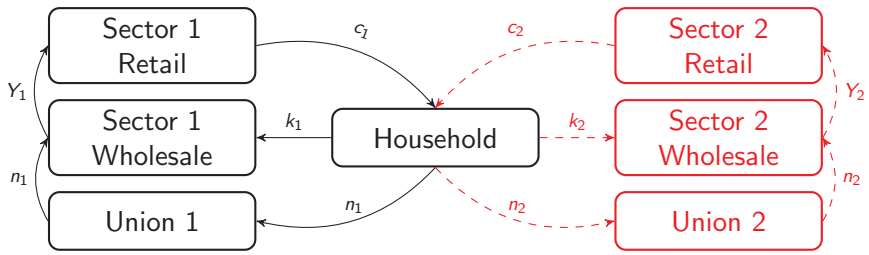

Sector 1 = Rest of the economy
Sector 2 = Leisure and Hospitality

Figure 1: The flowchart of the economy. Note: The figure reports in black (continuous line) the general sector and in red (dotted line) the pandemic sensitive sector. The arrows represent the flow of the indicated variables. Y_1 and Y_2 are the goods produced in the two sectors; k_1 and k_2 represent the capital stocks that are rented by the household to the two sectors; n_1 and n_2 are the hours of work supplied by the household to the two sectors; c_1 and c_2 denotes the household's consumption of the goods supplied by the two sectors.

function in the two sectors ($u_{k_1,t}$ and $u_{k_2,t}$) to maximize lifetime utility:

$$\mathbb{E}_0 \sum_{t=0}^{\infty} \beta^t a_{\zeta,t} \left[\frac{1-h_1}{1-\beta h_1} \log\left(c_{1,t} - h_1 c_{1,t-1}\right) + a_{j,t} \frac{1-h_2}{1-\beta h_2} \log\left(c_{2,t} - h_2 c_{2,t-1}\right) - \phi_{1,t} \frac{n_{1,t}^{1+\nu_1}}{1+\nu_1} - \phi_{2,t} \frac{n_{2,t}^{1+\nu_2}}{1+\nu_2} \right]. \tag{1}$$

Where h_1 and h_2 are the external habits parameters, $a_{\zeta,t}$ is the discount factor shock, $a_{j,t}$ is the $\mathcal{S}_2$ good preference shock, which affects the relative utility of the two products, and $\phi_{1,t}$ and $\phi_{2,t}$ are the labor supply shocks in the two sectors. These four shocks play a relevant role as exogenous determinants of potential large unexpected economic losses caused by the pandemic: the larger positive shocks to $\phi_{1,t}$ and $\phi_{2,t}$ reflect a significant increase in labor disutility due to health reasons; a large negative shock to $a_{j,t}$ will reduce the relative utility of consumption of goods from the pandemic-affected sector, $\mathcal{S}_2$; finally, a large negative shock to $a_{\zeta,t}$ affects the general intertemporal preferences and reflects the desire to postpone consumption of both goods.

The maximization is conducted subject to the sequence of budget constraints expressed in real terms as:

$$\begin{aligned} c_{1,t} + p_{2,t} c_{2,t} + k_{1,t} + p_{2,t} k_{2,t} + b_t = {} & \left(\frac{R_{t-1} b_{t-1}}{\pi_{1,t}} \right) + \left(\frac{w_{1,t} n_{1,t}}{X_{w_1,t}} \right) + \left(p_{2,t} \frac{w_{2,t} n_{2,t}}{X_{w_2,t}} \right) \\ & + k_{1,t-1} \left(1 - \delta_{k_1} + u_{k_1,t} r_{k_1,t}\right) \\ & + p_{2,t} k_{2,t-1} \left(1 - \delta_{k_2} + u_{k_2,t} r_{k_2,t}\right) + \Pi_t - \Psi_t. \end{aligned} \tag{2}$$

In the budget constraint, the variables $r_{k_1,t}$ and $r_{k_2,t}$ are the rental rates of capital in $\mathcal{S}_1$ and $\mathcal{S}_2$, while $w_{1,t}$ and $w_{2,t}$ are the wage rates. The parameters δ_{k_1} and δ_{k_2} are the capital

depreciation rates in the two sectors. The variable b_t represents government bonds with nominal gross return equal to R_t. The gross inflation rate of the numeraire, $P_{1,t}/P_{1,t-1}$, is denoted by $\pi_{1,t}$, while the relative price of the second final good in terms of the first, $P_{2,t}/P_{1,t}$, by $p_{2,t}$. The terms $X_{w_1,t}$ and $X_{w_2,t}$ are the wedge between the wage paid by the wholesale firms and the wage received by the household, which are collected by labor unions that are responsible for enforcing monopolistic competition in the labor market. In the budget constraint, Π_t collects all the profits from retailers and labor unions; these profits enter as a lump sum in the household's budget constraint, and their expression is provided in Appendix A. The variable Ψ_t collects the capital adjustment costs and utilization adjustment costs, see Appendix A. The first order conditions are standard and reported in Appendix A.

Firms

Similarly to Bernanke et al. (1999), we distinguish between competitive wholesale firms that produce intermediate goods and charge flexible wholesale prices, and retail firms that differentiate the final goods. The wholesale firm rents capital from households and labor from unions, taking the input prices as given to maximize the profit function expressed in real terms:

$$\max \frac{Y_{1,t}}{X_{1,t}} + p_{2,t}\frac{Y_{2,t}}{X_{2,t}} - \sum_{i=1,2}\left[\left(\frac{P_{i,t}}{P_{1,t}}\right) w_{i,t}n_{i,t} + \left(\frac{P_{i,t}}{P_{1,t}}\right) r_{k_i,t}u_{k_i,t}k_{i,t-1}\right],$$

subject to the production technologies:

$$Y_{1,t} = (a_{z_1,t}n_{1,t})^{1-\alpha_1}\,(u_{k_1,t}k_{1,t-1})^{\alpha_1}, \qquad Y_{2,t} = (a_{z_2,t}n_{2,t})^{1-\alpha_2}\,(u_{k_2,t}k_{2,t-1})^{\alpha_2}.$$

Above, $X_{1,t} = \frac{P_{1,t}}{P^w_{1,t}}$ is the markup between the wholesale price $P^w_{1,t}$ and the final goods price $P_{1,t}$ and $X_{2,t} = \frac{P_{2,t}}{P^w_{2,t}}$ is the markup between the wholesale price $P^w_{2,t}$ and $P_{2,t}$. The variables $a_{z_1,t}$ and $a_{z_2,t}$ represent labor productivity of both sectors. Since a pandemic is likely to impede the possibility of using labor to produce goods in a safe way, we allow labor productivity to be subject to large shocks.

Retailers buy intermediate goods $Y_{1,t}$ and $Y_{2,t}$ from wholesale firms at prices $P^w_{1,t}$ and $P^w_{2,t}$ and differentiate them at no cost into a continuum of varieties with constant elasticity

of substitution equal to ϵ_{π_1} and ϵ_{π_2}, respectively. The resulting demand for each variety j of final good is then given by $Y_{1,t}(j) = \left(\frac{P_{1,t}(j)}{P_{1,t}}\right)^{-\epsilon_{\pi_1}} Y_{1,t}$ and $Y_{2,t}(j) = \left(\frac{P_{2,t}(j)}{P_{2,t}}\right)^{-\epsilon_{\pi_2}} Y_{2,t}$. Retailers face quadratic adjustment costs *à la* Rotemberg in the retail prices $P_{1,t}(j)$ and $P_{2,t}(j)$, and these adjustment costs depend on last quarter inflation (with relative weights given by the indexation parameters ι_{π_1} and ι_{π_2}). The adjustment costs ($AC_{\pi_1,t}$ and $AC_{\pi_2,t}$) generate price stickiness and are given by the following expression:

$$AC_{\pi_i,t} = \frac{\eta_i}{2}\left(\frac{P_{i,t}(j)}{P_{i,t-1}(j)} - \pi_{i,t-1}^{\iota_{\pi_i}}\right)^2,$$

which shows that deviations of the prices of individual varieties $\left(\frac{P_{i,t}(j)}{P_{i,t-1}(j)}\right)$ from the the aggregate inflation ($\pi_{i,t-1}^{\iota_{\pi_i}}$) are penalized, depending on the rigidity parameters η_i. The price setting problem is standard, so we report it in Appendix A.

Unions

Unions buy homogeneous labor services from the households and differentiate them at no cost. Differentiated labor varieties are then aggregated back into CES composites which are sold to the wholesale firms. Labor unions face the demand schedules $n_{i,t}(h) = \left(\frac{W_{i,t}(h)}{W_{i,t}}\right)^{-\epsilon_w} n_{i,t}$, $i \in \{1,2\}$ for each individual variety of labor h, and pay quadratic adjustment costs *à la* Rotemberg for wage changes. The quadratic adjustment costs depend on previous quarter inflation with weights given by the indexation parameters ι_{w_1} and ι_{w_2}. These adjustment costs ($AC_{w_1,t}$ and $AC_{w_2,t}$) generate wage stickiness and are given by the following expression:

$$AC_{w_i,t} = \frac{\eta_{w_i}}{2}\left(\frac{W_{i,t}(h)}{W_{i,t-1}(h)} - \pi_{i,t-1}^{\iota_{w_i}}\right)^2,$$

where η_{w_i} is the degree of wage stickiness in sector i. The solution to this optimization problem gives the wage Phillips curves for the two sectors; the complete derivations are reported in Appendix A.

Monetary Policy

The central bank faces a ZLB constraint on the nominal interest rate r_t. This is particularly realistic in the context of the accommodating monetary policy reactions to the COVID-19

induced shocks. Following Dewachter and Wouters (2014) and Benigno et al. (2020), to combine the higher-order solution with the presence a ZLB, and to constrain the gross nominal interest rate above unity, we assume that the central bank has the following rule:

$$R_t = c_0 + c_1 R_{unc,t} + c_2 R_{unc,t}^2. \tag{3}$$

The coefficients c_0, c_1 and c_2 are obtained by fitting the barrier polynomial (see Appendix G) to the ideal piecewise linear function:

$$R_t = max\left\{1, R_{unc,t}\right\}. \tag{4}$$

where the unconstrained interest rate $R_{unc,t}$ is set by the Taylor rule:

$$R_{unc,t} = R_{unc,t-1}^{r_R} R_{ss}^{1-r_R} \pi_t^{(1-r_R)r_\pi} \left(\frac{GDP_t}{GDP_{t-1}}\right)^{(1-r_R)r_Y} \left(\frac{\exp(\varepsilon_{e,t})}{a_{s,t}}\right). \tag{5}$$

In the Taylor rule (5), $a_{s,t}$ represents an autocorrelated term reflecting persistent changes in the desired target of monetary policy, while $\varepsilon_{e,t}$ captures temporary deviations.

Modeling the ZLB as described in Equation (3) and (4) preserves nonlinearity in the model solution within the conventional and unconventional monetary policy regimes. The alternative route is to use piecewise-linear approximations inside each of the two regimes.

Aggregation and Equilibrium

The aggregate inflation rate is given by the weighted average of the inflation rates in the two sectors:

$$\pi_t = \pi_{1,t}^{\left(\frac{Y_{1,t}}{Y_{1,t}+p_{2,t}Y_{2,t}}\right)} \pi_{2,t}^{\left(\frac{p_{2,t}Y_{2,t}}{Y_{1,t}+p_{2,t}Y_{2,t}}\right)}.$$

Aggregate production is given by:

$$GDP_t = Y_{1,t} + p_{2,t}Y_{2,t}.$$

The evolution of the relative price of $\mathcal{S}_2$ is linked to the inflation rates in the two sectors:

$$\frac{p_{2,t}}{p_{2,t-1}} = \frac{\pi_{2,t}}{\pi_{1,t}}.$$

The model is closed with the resource constraints for the two goods, which also include all deadweight losses due to adjustment costs:

- Resource constraint for S_1:

$$\begin{aligned} &c_{1,t} + k_{1,t} - (1-\delta_{k_1})\, k_{1,t-1} + p_{2,t} k_{2,t} + p_{2,t}\,(1-\delta_{k_2})\, k_{2,t-1} \\ &= Y_{1,t}\left[1 - \frac{\eta_{\pi_1}}{2}\left(\pi_{1,t} - \pi_{1,t-1}^{\iota_{\pi_1}}\right)^2\right] - \frac{\eta_{w_1}}{2}\left(\omega_{1,t} - \pi_{1,t-1}^{\iota_{w_1}}\right)^2 w_{1,t}\, n_{1,t} - \Psi_t. \end{aligned} \tag{6}$$

- Resource constraint for S_2:

$$c_{2,t} = Y_{2,t}\left[1 - \frac{\eta_{\pi_2}}{2}\left(\pi_{2,t} - \pi_{2,t-1}^{\iota_{\pi_2}}\right)^2\right] - \frac{\eta_{w_2}}{2}\left(\omega_{2,t} - \pi_{2,t-1}^{\iota_{w_2}}\right)^2 w_{2,t} n_{2,t}. \tag{7}$$

The two resource constraints (6) and (7) ensure that the amount of consumption, investment and adjustment costs are equal to production. Given that $\mathcal{S}_2$ is identified as the US Leisure and Hospitality industry in the data, we postulate that investment goods are solely obtained out of $\mathcal{S}_1$ production. By Walras's law, the model can be formulated either with the two resource constraints or with one resource constraint coupled with the household's budget constraint (2), producing the exactly equal results.

Exogenous Processes

The persistent exogenous processes are described by equations (8)-(9). The steady state of the intratemporal utility shock to $\mathcal{S}_2$ consumption, j^{ss}, the steady state of the labor supply shock to $\mathcal{S}_1$, ϕ_1^{ss}, and the steady state of the labor supply shock to $\mathcal{S}_2$, ϕ_2^{ss} are calibrated as to match the ratios of hours worked in the two sectors and the relative price of the two goods, precisely:

$$\log(a_{z_1,t}) = \rho_{z_1}\log(a_{z_1,t-1}) + \varepsilon_{z_1,t}, \tag{8}$$

$$\begin{aligned} \log(a_{z_2,t}) &= \rho_{z_2}\log(a_{z_2,t-1}) + \varepsilon_{z_2,t}, \\ \log(a_{j,t}) &= (1-\rho_j)\log(j^{ss}) + \rho_j \log(a_{j,t-1}) + \varepsilon_{j,t}, \\ \log(a_{s,t}) &= \rho_s \log(a_{s,t-1}) + \varepsilon_{s,t}, \\ \log(a_{\zeta,t}) &= \rho_\zeta \log(a_{\zeta,t-1}) + \varepsilon_{\zeta,t}, \\ \log(\phi_{1,t}) &= (1-\rho_{\phi_1})\log(\phi_1^{ss}) + \rho_{\phi_1}\log(\phi_{1,t-1}) + \varepsilon_{\phi_1,t}, \\ \log(\phi_{2,t}) &= (1-\rho_{\phi_2})\log(\phi_2^{ss}) + \rho_{\phi_2}\log(\phi_{2,t-1}) + \varepsilon_{\phi_2,t}. \end{aligned} \tag{9}$$

3 Large Shocks and Model Solution

The model described in Section 2 enriched with large shocks and ZLB becomes a non-linear, non-Gaussian model. Subsection 3.1 introduces large shocks into the model, and

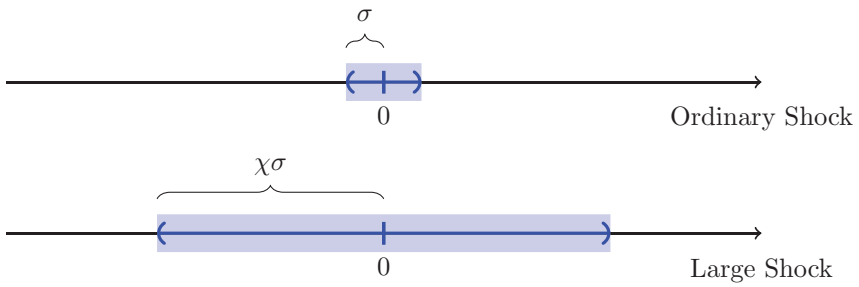

Figure 2: The modelization of large shocks. Note: The upper panel reports the ordinary shock centered at 0 and with a standard deviation equal to σ. The bottom panel reports the large shock with an inflated standard deviation equal to $\chi\sigma$. The factor of increase in variability is calibrated to $\chi = 10$.

Subsection 3.2 discusses model solution and nonlinearity.

3.1 Non-Gaussianity

The model outlined in Section 2 represents a nonlinear system of rational expectations, which is driven by the following vector of structural shocks:

$$\boldsymbol{\varepsilon}_t = \left[\varepsilon_{z_1,t}, \varepsilon_{z_2,t}, \varepsilon_{j,t}, \varepsilon_{\zeta,t}, \varepsilon_{\phi_1,t}, \varepsilon_{\phi_2,t}, \varepsilon_{s,t}, \varepsilon_{e,t}\right]'. \tag{10}$$

We allow the first six innovations to (possibly) display large shocks. To exclude extreme policy rate movements that are not related to changes in prices and real activity, we do not allow large shocks to occur for the two monetary policy innovations: $\varepsilon_{s,t}$ (the shock associated with a persistent deviation from the target policy rate), and $\varepsilon_{e,t}$ (the shock associated with a temporary deviation from the target policy rate). The modelling of large shocks is a challenging task, as the rarity of the events involved prevents us from observing large enough samples to estimate their characteristics.[4] The strategy that we adopt is agnostic and accommodates the possibility of very different scenarios. In particular, we assume that each of the six shocks in our model can be drawn from either a zero mean Normal distribution with ordinary standard deviation σ_i (ordinary component) or a zero mean Normal distribution with an inflated standard deviation equal to $\chi\sigma_i$ (large shock component). A graphical representation is provided in Figure 2.

[4] Gourio (2012) and Andreasen (2012b) have both suggested using an ordinary component and a rare shock component in the DSGE framework. The focus of their calibrated models is explaining how the risk of rare disasters in technology can impact risk premia. Rather than assessing the risk of a rare shock's prospective realization, we are more interested in examining the event of a rare shock that has actually occurred.

The large shock scaling parameter χ is calibrated to provide a reasonable and agnostic range for the magnitude of the shocks responsible for the pandemic-related disruption ($\chi = 10$). Since the first six shocks in equation (10) can have either an ordinary or an inflated standard deviation, we must consider 2^6 combinations of possible ordinary/inflated shocks.[5] In each time period, we denote with ψ_t the probability that at least one large shock occurs (ex-ante large shock probability). In this case the (standardized) vector of shocks ($\tilde{\varepsilon}_t \equiv \frac{\varepsilon_t}{\sigma}$) can be represented as a Gaussian mixture:

$$p(\tilde{\varepsilon}_t) = \left(1 - \sum_{k=1}^{K} \psi_{k,t}\right) \mathcal{N}(0, I) + \sum_{k=1}^{K} \psi_{k,t} \mathcal{N}(0, \Omega_k), \tag{11}$$

where K is the number of combinations with at least one large shock ($K = 63$); $\psi_{k,t}$ is ex-ante probability of the k-th combination realizing at time t; and Ω_k is a diagonal covariance matrix where each element is one $\left(\chi^2\right)$ in correspondence with shocks that are ordinary (large) in the k-th component.[6] We assume a priori equiprobability for all the sixty-three large shocks combinations, precisely, $\psi_{k,t} = \psi_t/63$, where ψ_t is the scalar time-varying ex-ante large shock probability. We do not fix ψ_t, but we estimate it together with the DSGE parameters assuming it is a step function, low before the pandemic and high afterward, see Section 6. Our filter in Section 6 will exploit the representation of the Gaussian mixture in equation (11) to obtain the ex-post probability of the realized combination of shocks given the observed data. Similarly to Lenza and Primiceri (2022), we also show in Section 7.5 that to estimate the model parameters without bias, it is important to take into account the inflated variance of the shocks during the pandemic. Unlike Lenza and Primiceri (2022) who select a priori the quarters when large shocks occur and estimate the inflated variability, we fix the inflated variability (χ) and estimate the quarters when the shocks

[5] We have 63 combinations where there are at least one large shock and one combination where all shocks have the ordinary standard deviation.

[6] Alternatively, it is possible to express the distribution of the shocks by using an auxiliary random vector S_t that determines the variance parameters of the shocks. S_t is a vector of indicator variables of the same dimension of the structural shocks. Each entry $S_{i,t}$ in the vector S_t is equal to 0 (1) if the corresponding shock is ordinary (large). This means that:

$$p(\tilde{\varepsilon}_t | S_t) = \prod_{i=1}^{n_\varepsilon} \mathcal{N}\left(0, (1 - S_{i,t}) + S_{i,t}\chi^2\right),$$

and

$$p(S_t) = \begin{cases} (1 - \sum_{k=1}^{K-1} \psi_{k,t}), & \text{if } S_t = [0, ..., 0]'. \\ \psi_{k,t}, & \text{otherwise.} \end{cases}$$

occur. In addition, our filter allows us to identify the combination of large shocks that materialize and provide an economic interpretation of pandemic shocks.

Finally, Cúrdia et al. (2014) and Chib and Ramamurthy (2014) use a Student's t distribution to model large shocks. We could use their approach, but it would not be optimal for several reasons. First, given the large realization of pandemic shocks, we need a Student's t with 2 degrees of freedom that could generate extreme shocks like the ones experienced during the pandemic. In particular, Student's t distribution with two degrees of freedom ($df = 2$) could generate draws outside the 10 standard deviation interval with a probability of 1%. In Section 7.5 and in Appendix E we show that this would lead to an unbonded variance. Second, using the Student's t distribution does not handle the presence of multiple large shocks in the same quarter, something that is possible with the mixture in formula (11). Finally, using a Gaussian Mixture allows us to use the Cubature formula (see Arasaratnam and Haykin, 2009 and Section 4) which is not possible with a Mixture of Student's t.

3.2 Nonlinearity

To account for higher-order effects in the transmission of large shocks and the ZLB, the optimality conditions of the model are approximated nonlinearly. Indeed, a first-order approximation would neglect the interaction terms in the transmission of shocks, an undesirable feature in our large shock framework. Secondly, the smooth ZLB described in Section 2 would be completely missed by a linear approximation, as shown in Figure 3. To estimate the model in a reasonable amount of time, a fast solution method is needed,

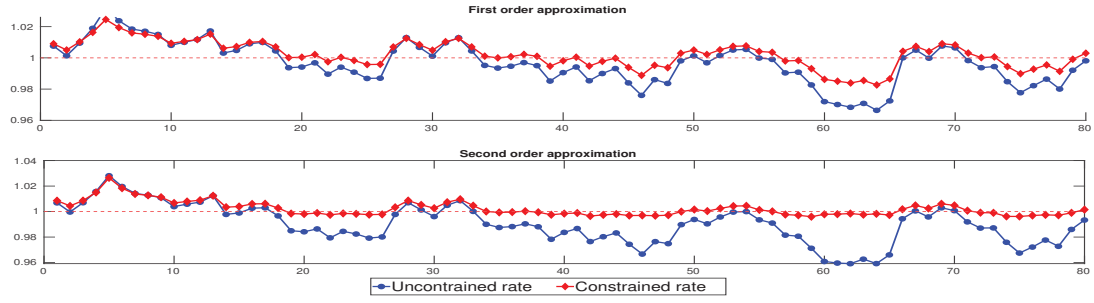

Figure 3: First and second order approximation. Note: The figure reports a simulation of the unconstrained and constrained interest rates using the smooth barrier polynomial, see Section 2, at the first and second order, for a given sequence of shocks. The blue (circle) line is the unconstrained interest rate, while the red (diamond) line is constrained rate. In the first order approximation the constrained rate would be allowed to substantially cross the lower bound, whereas in the second order approximation it is effectively constrained.

therefore we follow Levintal (2017) and use a second-order perturbation. The solution is computed around the non-stochastic steady state, which is derived in Appendix D.

The model solution gives:

$$\begin{aligned} x_t^C &= g\left(x_t^S;\theta\right), \\ x_{t+1}^S &= h\left(x_t^S;\theta\right) + R\left(\theta\right)\tilde{\varepsilon}_{t+1}, \end{aligned} \tag{12}$$

where: x_t^S are the model states; x_t^C are the model controls; R is the matrix that links the standardized shocks to the model states; and θ is the parameters vector. The nonlinearity originates from the second-order polynomials in the economic states ($g(\cdot)$ and $h(\cdot)$). [7]

The model variables are linked to the observable data through the measurement equations:

$$\mathbf{y}_t = A + B\mathbf{x}_t + u_t, \qquad u_t \sim \mathcal{N}(0, H), \tag{13}$$

where: $\mathbf{y}_t$ are the observed series; $\mathbf{x}_t = \left[x_t^{S'}\, x_t^{C'}\right]'$ is the stacked vector of the economic states and controls; and u_t are the measurement errors. As Herbst and Schorfheide (2015) describe when the number of series is greater than the number of structural shocks, we need to add measurement erros to avoid stochastic singularity. In our empirical application, see Section 7, we have 11 series and 8 structural shocks so we need to add the measurement errors, u_t. We assume that H is diagonal and that it has a standard deviation equal to 15% of the variability of the corresponding data series, see Aruoba et al. (2021). In this calculation, we exclude the pandemic quarters to avoid over-inflating the measurement errors variance.

4 Filtering the Nonlinear DSGE with large shocks

Given the model parameters θ, the state-space representation described in equations (12) and (13) implicitly defines the transition and measurement densities $p\left(\mathbf{x}_t|\mathbf{x}_{t-1};\theta\right)$ and $p\left(\mathbf{y}_t|\mathbf{x}_t;\theta\right)$, from which the joint distribution of unobserved states and observations can

[7] The model solution by Levintal (2017) in equation (12) closely follows Schmitt-Grohé and Uribe (2004) and is numerically equivalent to the one performed by Dynare, see Adjemian et al. (2022). Also note that the model states (x_{t+1}^S) depend nonlinearly on the structural shocks ($\tilde{\varepsilon}_t$) through the function $h(\cdot)$.

be constructed:

$$p\left(\mathbf{x}_{1:T}, \mathbf{y}_{1:T}|\theta\right) = \prod_{t=1}^{T} p\left(\mathbf{x}_t|\mathbf{x}_{t-1};\theta\right) p\left(\mathbf{y}_t|\mathbf{x}_t;\theta\right). \tag{14}$$

By recursively integrating the unobserved states from the joint density in (14), the likelihood function can be computed by prediction error decomposition:

$$p\left(\mathbf{y}_{1:T}|\theta\right) = \prod_{t=1}^{T} p\left(\mathbf{y}_t|\mathbf{y}_{1:t-1};\theta\right). \tag{15}$$

In non-Gaussian nonlinear state-space models, the densities appearing in equations (14) and (15) do not have closed-form solutions. To deal with this problem, approximation methods such as deterministic integration filters (our choice) or simulation methods (PFs) must be used.

Since the seminal paper of Gordon et al. (1993), PFs have been used in non-linear DSGE models; see An and Schorfheide (2007), Fernández-Villaverde and Rubio-Ramírez (2007), Fernández-Villaverde et al. (2011) and Flury and Shephard (2011).

Unfortunately, PFs suffer from the curse of dimensionality, as they require an exponentially increasing number of particles, see Bengtsson et al. (2008). For this reason, PFs entail a high computational burden, even for medium-sized models like ours. To overcome this problem, different solutions have been proposed. Among others, Liu and Chen (1998) propose the Conditionally Optimal Particle Filter (COPF), whose effectiveness in the context of DSGE estimation has been shown by Herbst and Schorfheide (2015) and Aruoba et al. (2021). Except for special cases (see Creal, 2017), closed-form expressions for the conditionally optimal density used by the COPF are difficult to derive or not available. In these cases, a possible alternative is the Approximate Conditionally Optimal Particle Filter (ACOPF), a PF that approximates the unknown optimal proposal density; an example of the ACOPF is derived in Appendix F.

The presence of large shocks represents an additional blow to the effectiveness of PFs. Large shocks require a huge number of particles to describe all possible outcomes that can occur after a disaster even stronger than those generated after the 2008 crisis, see Pitt and Shephard (1999) and Amisano and Tristani (2011). The problem associated with outliers in the observations was also highlighted by Herbst and Schorfheide (2015), who showed that data related to the Great Recession challenge the effectiveness of PFs

in the estimation of DSGE models. In this respect, it is worth noticing that COVID-19 has created unprecedented movements in the time series. Unlike the PFs, the Sigma point filters (SPFs) assume a convenient parametric form for the density in the Bayesian filtering recursion and replace the particles of simulation-based methods with a small set of (deterministic) selected points that are used to calculate, recursively, the moments of the density. A textbook treatment of the SPF can be found in Särkkä (2013). They have also been applied to estimate of nonlinear DSGE, see among others Andreasen (2012a, 2013), Ivashchenko (2014), Kollmann (2015), Binning and Maih (2015), Noh (2020) and Benigno et al. (2020). While these filters are approximated by construction, Andreasen (2013) and Kollmann (2015) show that they can outperform PFs.

5 Mixture of Mixture of Cubature Kalman Filter

To deal efficiently with the nonlinear and non-Gaussian state-space models with (possibly) large shocks, we propose a new filter, in the family of Gaussian Sum Filters (GSFs), that tests all the possible large shocks and handles nonlinearity at the same time. Our filter is a Mixture of Mixture of Cubature Kalman Filter (MM-CKF) that requires much less computational time than the PFs. GSFs, also known as Gaussian mixture filters, were first introduced in the signal processing literature by Sorenson and Alspach (1971) and Alspach and Sorenson (1972). These filters represent the prediction and filtering densities of unobserved states as Normal mixtures. In the case of filtering densities:

$$\begin{aligned} p\left(\mathbf{x}_{t-1}|\mathbf{y}_{1:t-1}\right) &\approx \sum_{g=1}^{G_{t-1}} p\left(\mathbf{x}_{t-1}|\kappa_t^g, \mathbf{y}_{1:t-1}\right) p\left(\kappa_{t-1}^g|\mathbf{y}_{1:t-1}\right) \\ &= \sum_{g=1}^{G_{t-1}} \mathcal{N}\left(m_{t-1|t-1}^g, P_{t-1|t-1}^g\right) w_{t-1|t-1}^g, \end{aligned} \tag{16}$$

where G_{t-1} is the number of the mixture components, κ_{t-1}^g is an indicator variable and $w_{t-1|t-1}^g$ are the corresponding weights at time $t-1$. GSFs share the idea that any probability density arising from, e.g. nonlinearity, can be approximated with arbitrary precision by a weighted sum of Gaussian densities (Alspach and Sorenson, 1972). The first two moments $m_{t-1|t-1}^g$ and $P_{t-1|t-1}^g$ of each component are recursively estimated by filters running in parallel. Parallel Kalman filters, Extended Kalman filters, Particle

filters, Unscented Kalman filters, Cubature Kalman filters have been used by Sorenson and Alspach (1971), Alspach and Sorenson (1972), Kotecha and Djuric (2003), Faubel et al. (2009) and Leong et al. (2013). In the prediction step, our filter has two mixtures, the first for the nonlinearity generated by e.g. the ZLB, the second for the inflated error variance according to equation (11). For each of the component in the filtering density in equation (16), K predictions are formed:

$$\begin{aligned} p\left(\mathbf{x}_t|\mathbf{y}_{1:t-1}\right) &\approx \sum_{g=1}^{G_{t-1}} \sum_{k=1}^{K} p\left(\mathbf{x}_t|\kappa_t^{g,k}, \mathbf{y}_{1:t-1}\right) p\left(\kappa_t^{g,k}|\mathbf{y}_{1:t-1}\right) \\ &= \sum_{g=1}^{G_{t-1}} \sum_{k=1}^{K} \mathcal{N}\left(m_{t|t-1}^{g,k}, P_{t|t-1}^{g,k}\right) w_{t|t-1}^{g,k}, \end{aligned}$$

where: the mixture over G_{t-1} handles the nonlinearity in the policy function; the mixture over K handles the different components of the over-inflated variance, see equation (11); and $w_{t|t-1}^{g,k}$ stands for $w_{t-1|t-1}^{g}\psi_{k,t-1}$. To deal with nonlinearity and non-Gaussianity contemporaneously, we have a splitting and a merging step. In the first, each of the G_{t-1} filtering densities, that handle non-linearity, are divided into as many components as those that make up the noise mixture $p(\tilde{\boldsymbol{\varepsilon}}_{t-1}) = \sum_{k=1}^{K} \psi_{k,t-1} p\left(\boldsymbol{\varepsilon}_{t-1}^{k}\right)$. Since, for each of the G_{t-1} components, new K filters are created, an exponentially increasing number of densities arises. The merging step avoids this degeneration using a collapsing strategy that constantly retains the components with the highest weights in each iteration t, as suggested by Kotecha and Djuric (2003). In each iteration, our filter allows at most $\bar{G}$ components, namely $G_t \leq \bar{G}$.[8] Note that the proposed filter encompasses the CKF when $\bar{G} = 1$ and $K = 1$.

A sketch of the MM-CKF is provided below (Algorithm 1), while a detailed description is reported in Appendix B.

[8] Precisely, $G_t = \min\{\bar{G}, G_{t-1}K\}$, except when some components have negligible weights and are discarded, see Appendix B.

Algorithm 1 Sketch of the MM-CKF filter.

1: **for** $t = 1$ to T **do**

2: The filtering density of unobserved states is approximated by $p\left(\mathbf{x}_{t-1}|\mathbf{y}_{1:t-1}\right) = \sum_{g=1}^{G_{t-1}} \mathcal{N}\left(m_{t-1|t-1}^{g}, P_{t-1|t-1}^{g}\right) w_{t-1|t-1}^{g}$.

3: **for** $g = 1$ to G_{t-1} **do**

4: **for** $k = 1$ to K **do**

5: Use the **CKF** to update mean $m_{t|t}^{g,k}$, variance $P_{t|t}^{g,k}$ and weight $w_{t|t}^{g,k}$ of the $\{g^{th}, k^{th}\}$ mixand, assuming noise is coming from the k^{th} component.

6: **end for**

7: **end for**

8: Reduce the number of mixands if $G_{t-1}K > \bar{G}$ or if some weight is negligible.

9: **end for**

In Algorithm 1, the last period filtered unobserved components (line 2):

$$p\left(\mathbf{x}_{t-1}|\mathbf{y}_{1:t-1}\right) = \sum_{g=1}^{G_{t-1}} \mathcal{N}\left(m_{t-1|t-1}^{g}, P_{t-1|t-1}^{g}\right) w_{t-1|t-1}^{g},$$

provide estimates on the unobserved states. For each of the G_{t-1} filtered components that form the filtered density and for each of the K components that form the state noise, the algorithm uses the CKF formulae (line 5). This allows us to compute the predicted mean $m_{t|t-1}^{g,k}$ and the covariance $P_{t|t-1}^{g,k}$ for the unobserved states supposing that noise comes from the k^{th} component. The density of predicted unobserved states, for each shock combination, is then approximated by:

$$p\left(\mathbf{x}_t|\mathbf{y}_{1:t-1}, \kappa_t^{g,k}\right) = \mathcal{N}\left(m_{t|t-1}^{g,k}, P_{t|t-1}^{g,k}\right), \quad g = 1, \ldots, G_t, \quad k = 1, \ldots, K.$$

The predicted unobserved states are approximated by the ensemble density:

$$p\left(\mathbf{x}_t|\mathbf{y}_{1:t-1}\right) = \sum_{g=1}^{G_{t-1}} \sum_{k=1}^{K} \mathcal{N}\left(m_{t|t-1}^{g,k}, P_{t|t-1}^{g,k}\right) w_{t|t-1}^{g,k},$$

where the predicted weights for each component are given by $w_{t|t-1}^{g,k} = w_{t-1|t-1}^{g}\psi_{k,t}$, for $k = 1, \ldots, K$. For each of the predicted components $G_{t-1}K$, use the CKF formulas to compute the predicted observations mean $\mathcal{Y}_{t|t-1}^{g,k}$, the predicted observations covariance

$\mathcal{F}_{t|t-1}^{g,k}$ and the predicted variance-covariance between unobserved states and observations $\mathcal{P}_{t|t-1}^{g,k,\mathbf{xy}}$. With these quantities, the CKF updating is performed using the new observation $\mathbf{y}_t$ in order to obtain the new filtered means $m_{t|t}^{g,k}$ and covariances $P_{t|t}^{g,k}$ for unobserved states. Weights are then updated using the Bayes rule:

$$w_{t|t}^{g,k} = \frac{w_{t|t-1}^{g,k}\mathcal{N}\left(\mathbf{y}_t; \mathcal{Y}_{t|t-1}^{g,k}, \mathcal{F}_{t|t-1}^{g,k}\right)}{\sum_{g=1}^{G_{t-1}}\sum_{k=1}^{K} w_{t|t-1}^{g,k}\mathcal{N}\left(\mathbf{y}_t; \mathcal{Y}_{t|t-1}^{g,k}, \mathcal{F}_{t|t-1}^{g,k}\right)}.$$

To avoid an exponential proliferation of the number of components, a collapsing strategy is performed for the number of mixands (line 8), as detailed in Appendix B. More specifically, components with negligible weights are removed from the mixture, and if the number of components exceeds the maximum of $\bar{G}$, then the most significant components are retained. Once these quantities have been computed, a new iteration of the filter can be run.

Our approach to non-Gaussianity is drawn from the engineering literature where a similar decomposition is used for nonlinear state estimation; see, among others, Pei et al. (2013) and Pei et al. (2014). Splitting rules based on Gaussian mixtures to treat large measurement errors or system noise have been employed in disparate branches of signal processing. In our specific case, the different components of the system noise originate from the various possible large economic shocks to be tested. The splitting rule is the direct translation, in the CKF framework, of the ones presented in Alspach and Sorenson (1972) for KFs and Kotecha and Djuric (2003) for PFs.

Splitting the filter into the K mixture components at each time t is a computationally costly operation that must be repeated over the millions of likelihood evaluations required by the SMC. To speed up computational times, we avoid splitting the filter when it is irrelevant. Indeed, a simple plot of the time series suggests that it is very unlikely to observe disaster shocks (e.g. COVID-19 type shocks) before 2020. At the same time, we do not want to completely exclude the possibility of detecting large shocks before the pandemic quarters. The filter, by construction, does not split when the estimated ex-ante probability of large shock ψ_t is too low (that is, $\psi_t < \bar{\psi} = 10^{-3}$). We stress that ψ_t is estimated endogenously together with the DSGE parameters and not fixed a priori. Specifically, we model the time-varying ex-ante probability of large shock ψ_t to be equal to ψ_{pre} before 2020 and equal to ψ_{post} thereafter. Imposing a time-varying ex-ante probability

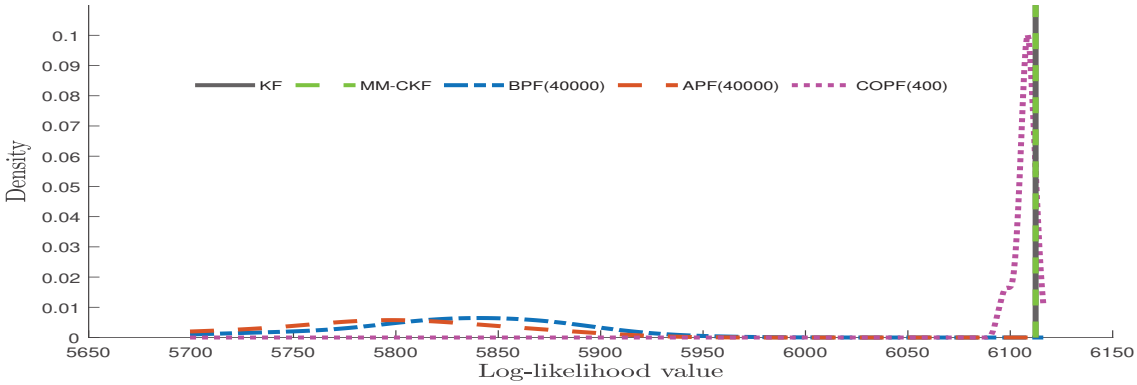

Figure 4: Density kernel estimates for $N = 100$ log-likelihood evaluations. Note: The considered filters are the Kalman Filter (KF), the Bootstrap Particle Filter (BPF), the Auxiliary Particle Filter (APF), the Conditionally Optimal Particle Filter (COPF) and the Mixture of Mixture Cubature Kalman Filter (MM-CKF). The vertical line reports the results for the KF (black vertical line) and the MM-CKF (green dotted vertical line). The BPF (blue dashed-dot line), APF (red dashed line), and COPF (purple dotted) have negative bias.

of large shock is crucial, as a fixed and relatively low one for the entire sample would make the pandemic quarters extremely influential in driving the likelihood function, thus biasing the estimates of the parameters to fit these observations (the predictive likelihood increments would drop massively for these data points), see Appendix E. We then estimate these two probabilities together with the structural parameters of the model by imposing truncated normal priors on the unit interval for them, see Table 3. Note that the modelling strategy of Lenza and Primiceri (2022) corresponds to the case in which the priors are degenerate and fixed at 0 before 2020 and to 1 thereafter.

6 Monte Carlo Experiments

To show that our filter can correctly identify the source of the shock and outperform PFs with a massively reduced running time (see also Andreasen, 2013 and Kollmann, 2015) we perform three simulation experiments. In the first experiment, we simulate $N = 100$ times the model described in Section 2 and we apply a first-order approximation to obtain a linear and Gaussian model. In this case, the KF is the optimal filter and gives an exact log-likelihood. Figure 4 reports the Monte Carlo results and shows that MM-CKF collapses to the exact KF while BPF, APF, and COPF have biased log-likelihoods (due to Jensen's inequality).

In the second experiment, we simulate $N = 100$ times the model in Section 2, we take a second-order approximation and finally add a random large (state) shock. The resulting

Table 1: RMSE of the Monte Carlo experiment for $N = 100$ replications of the Two-Sector model with large shocks. Note: The Table reports the full name (Full Name) with the associated symbol (Symbol). The filters are: Kalman filter (KF); Bootstrap Particle Filter with 40000 particles (BPF); Auxiliary Particle Filter with 40000 particles (APF); the Approximate Optimal Particle Filter with 400 and 4000 particles (ACOPF(400), ACOPF(4000)); and the Mixture of Mixture of Cubature Kalman Filter (MM-CKF) with four components ($\bar{G} = 4$).

Full Name	Symbol	KF	BPF	APF	ACOPF(400)	ACOPF(4000)	MM-CKF
Hours $\mathcal{S}_1$	n_1	0.39	0.44	0.46	0.48	0.39	0.20
Hours $\mathcal{S}_2$	n_2	2.60	1.90	1.70	2.00	1.90	0.84
Production $\mathcal{S}_1$	Y_1	3.40	0.93	1.10	1.10	1.10	1.00
Production $\mathcal{S}_2$	Y_2	2.50	1.90	1.70	2.10	1.90	0.99
Consumption $\mathcal{S}_1$	c_1	3.00	0.94	1.10	1.10	1.10	1.00
Consumption $\mathcal{S}_2$	c_2	2.60	1.90	1.70	2.10	1.90	1.00
Capital $\mathcal{S}_1$	k_1	4.30	1.10	1.30	1.40	1.20	1.10
Capital $\mathcal{S}_2$	k_2	2.30	2.50	2.40	2.60	2.50	2.60
Relative price	p_2	5.20	1.30	1.50	1.60	1.40	1.20
Inflation	π	0.04	0.04	0.04	0.02	0.01	0.01

Time in Seconds

KF	BPF	APF	ACOPF(400)	ACOPF(4000)	MM-CKF
0.064	610	1100	400	3400	7.9

model is nonlinear and non-Gaussian and the exact expression for the likelihood is not available. To compare the performances of MM-CKF with the other filters, we use the RMSE of the filtered (estimated) and the (simulated) latent state:

$$RMSE_{i,f} = \sqrt{\frac{1}{N}\sum_{j=1}^{N}\sum_{t=1}^{T}\left(\hat{\mathbf{x}}_{i,t|t}^{f} - \mathbf{x}_{i,t}^{s}\right)^2}.$$

where $\hat{\mathbf{x}}_{i,t|t}^{f}$ for $i = 1, \ldots, n$ and $\mathbf{x}_{i,t}^{s}$ for $i = 1, \ldots, n$ are the filtered and the simulated latent states, respectively. Table 1 reports a selection of the RMSE (the full table is in Appendix G) and the computing time (in seconds) for the KF, BPF with 40000 particles, APF with 40000 particle, ACOPF with 400 and 4000 particles, and the MM-CKF with $\bar{G} = 4$. Table 1 shows that the MM-CKF is much faster than BPF, APF and ACOPF. The KF is the fastest filter, but gives biased results. Overall, the results show that the MM-CKF is a valuable choice for filtering unknown latent states where computational time and robustness to large shocks are crucial.

In the third Monte Carlo experiment, we study whether the MM-CKF provides a good identification of large shocks. We simulate $N = 500$ times the model of Section 2 with the

parameters obtained from our empirical application, see Section 7. We then add negative (i.e., Realized Disaster as COVID-19 type shocks in 2020:Q2) and positive (i.e., Realized Rebound as the one realizing in 2020:Q3) shocks of similar type and intensity as those found in our empirical application. To simulate a sample close to the real data, the length of the simulated series is equal to $T = 148$, with a simulated disaster in $t = 142$ (equivalent to 2020:Q2) and a rebound in $t = 143$ (equivalent to 2020:Q3). Based on the number of observations ($T = 148$) and the number of simulations ($N = 500$) there are a total of 74000 data points. By design, we have 73000 normal observations, 500 realized disaster, and 500 realized rebound, which occur sequentially. Table 2 reports the Monte Carlo results and shows that the MM-CKF correctly detects the type and location of large shocks. The MM-CKF correctly selects ordinary shocks 99% of time, the location and combination of the disaster shock 95% of time, the location and combination of the rebound 97% of time, and finally the location and combination of both 92% of time.

In addition, in Figure 5 we report the log-likelihood contributions of each quarter, for three of the $K = 64$ shock combinations, zoomed around the disaster and rebound events. The three combinations are: the ordinary component (without large shocks); the realized disaster component in period $t = 142$; and the realized rebound component in period $t = 143$. As shown in the figure, the ordinary component (blue line) is the one with the highest probability before and after the disaster periods. In such quarters, the disaster and rebound components are correctly identified, with the highest likelihood of the realized disaster (red squared line) in $t = 142$ and the highest likelihood of the realized rebound (black circle line) in $t = 143$. For illustration, the figure also shows the component with a single labor supply shock (represented by the green diamond line), which consistently has a lower likelihood compared to the others.

We conclude this experiment with Figure 6, which provides a closer look at the disaster and rebound quarters, and shows the likelihood of all possible combinations ($K = 64$) in $t = 142$ and in $t = 143$. The realized disaster and rebound combinations are selected as those with the highest likelihood. The figure also reports the likelihood ratio of the realized disaster and rebound, showing that one combination has the highest weight, while the others have smaller or null weights.

Table 2: Shock type and location Monte Carlo results for $T = 148$ and $N = 500$ replications. Note: The table reports: the shock type (Shock type); the number of times it is present in the simulated dataset (Occurred); the number of times it is detected (Detected); and the results in percentage (Percentage). The possible outcome of the experiment are: normal observations (Ordinary), realized disaster (Disaster); realized rebound (Rebound), and realized disaster and rebound that occur sequentially (Dis. + Reb.)

Shock type	Occurred	Detected	Percentage
Ordinary	73000	72962	99%
Disaster	500	475	95%
Rebound	500	486	97%
Dis. + Reb.	500	462	92%

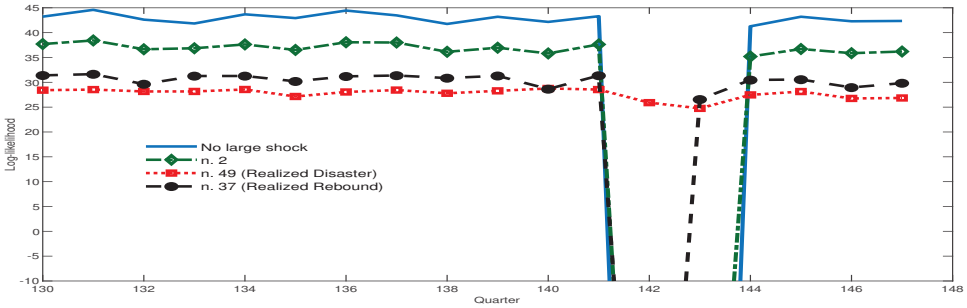

Figure 5: The log-likelihood contributions of each quarter in a sample with simulated large shocks. The Figure reports the log-likelihood contributions associated with four components among the $K = 64$ possible ones: the ordinary component (No large shock, blue continuous line); the component number two corresponding to a large shock to labor supply in $\mathcal{S}_1$ alone (Labor supply shock in $\mathcal{S}_1$, green diamond line); the component corresponding to the simulated realized disaster at time $t = 142$ (Realized Disaster, red squared line); the component corresponding to the simulated

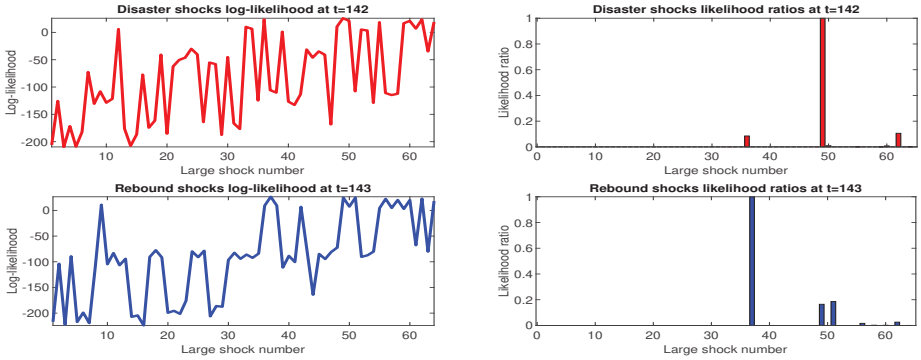

Figure 6: Log-likelihood and likelihood ratio for each of the possible $K = 64$ combinations at realized disaster ($t = 142$, upper plots) and realized rebound ($t = 143$, lower plots). Note: The left plots report the log-likelihood for all $K = 64$ possible combinations in the realized disaster (top left plot) and realized rebound (bottom left plot). The top right plot reports the ratio of the highest component with respect to the remaining components of the disaster shock. The lower right plot reports the ratio of the highest component with respect to the remaining ones for the rebound shock.

7 Empirical Analysis

7.1 Data

We estimate the model on US quarterly data from 1985:Q1 to 2021:Q4. Eleven model variables are linked to the data series: value-added in the general sector; value-added in the Leisure and Hospitality sector; aggregate investment; aggregate consumption; hours worked in the general sector; hours worked in the Leisure and Hospitality sector; price inflation in the general sector; price inflation in the Leisure and Hospitality sector; wage inflation in the general sector; wage inflation in the Leisure and Hospitality sector; and the Federal Funds Rate. Value-added, investment, consumption and hours worked in both sectors are in per capita terms and in demeaned growth rates; price and wage inflation are demeaned; the Federal Funds Rate is in level. A detailed description of the sources and construction of the data is provided in Appendix C. The sectoral value-added and inflation, retrieved from the Bureau of Economic Analysis (BEA), are available at annual frequencies before 2005 and quarterly frequencies after.[9]

7.2 Prior Specification

Following Del Negro and Schorfheide (2008), we divide the model parameters into three categories: steady-state parameters, $\Theta_{(\text{ss})}$; parameters related to the law of motions of endogenous variables, $\Theta_{(\text{endo})}$; and parameters associated with the law of motion of exogenous variables, $\Theta_{(\text{exo})}$:

$$\begin{aligned}
\Theta_{(\text{ss})} &= [\beta, \alpha_1, \alpha_2, \delta_{k_1}, \delta_{k_2}, \epsilon_{\pi_1}, \epsilon_{\pi_2}, \epsilon_{w_1}, \epsilon_{w_2}, j^{ss}, \phi_1^{ss}, \phi_2^{ss}, \nu_1, \nu_2]', \\
\Theta_{(\text{endo})} &= [r_R, r_Y, r_\pi, \iota_{\pi_1}, \iota_{\pi_2}, \iota_{w_1}, \iota_{w_2}, h_1, h_2, \eta_{\pi_1}, \eta_{\pi_2}, \eta_{w_1}, \eta_{w_2}, \eta_{u_1} \\
&\quad \eta_{u_2}, \eta_{k_1}, \eta_{k_2}]', \\
\Theta_{(\text{exo})} &= [\rho_{z_1}, \rho_{z_2}, \rho_j, \rho_{\phi_1}, \rho_{\phi_2}, \rho_\zeta, \rho_s, \sigma_{z_1}, \sigma_{z_2}, \sigma_j, \sigma_{\phi_1}, \sigma_{\phi_2}, \sigma_\zeta, \sigma_s, \sigma_e, \psi_{pre}, \psi_{post}]'.
\end{aligned}$$

Following standard practice in the literature on DSGE models (see, among others, Smets and Wouters, 2007), we fix a subset of the parameters to well-established values based on economic theory (all the parameters belonging to $\Theta_{(\text{ss})}$ are calibrated except the labor

[9] In case of data available at annual frequencies, we assume that we observe just one quarter per year, and the other three are missing. The missing values are handled as unobserved variables by MM-CKF, similarly to Durbin and Koopman (2012).

elasticity parameters ν_1 and ν_2, which are estimated). We set $\beta = 0.991$ to obtain a real annual interest rate of 3 percent in steady state. The elasticity of substitution for the two final goods and the labor varieties is set equal to $\epsilon_{\pi_1} = \epsilon_{\pi_2} = \epsilon_{w_1} = \epsilon_{w_2} = 1/0.15 + 1$ to imply steady-state markups of 15 percent. The quarterly capital depreciation rates are set at $\delta_{k_1} = \delta_{k_2} = 0.025$, to induce a steady-state investment to output ratio of 22 percent. Capital share parameters in technology are equal to $\alpha_1 = \alpha_2 = 0.35$, to match a labor share of income of 65 percent. We normalize the hours worked in sector $\mathcal{S}_1$ as $n_1 = 1$ and set the steady state of hours worked in sector $\mathcal{S}_2$ as $n_2 = 0.07$, to reflect the mean ratio of the hours worked in the two sectors as observed in the sample (see Appendix C for the data sources). We also target the mean relative price between sector $\mathcal{S}_2$ and the rest of the economy by imposing $p_2 = 0.78$ in the steady state.[10] These steady-state targets jointly imply fixing the steady state of intratemporal utility and labor supply shocks to $j^{ss} = 0.0715$ (which is the ratio between households' expenditure on $\mathcal{S}_2$ goods over $\mathcal{S}_1$ goods, see Appendix D), $\phi_1^{ss} = 0.643$ and $\phi_2^{ss} = 1.896$, respectively. Details on derivations of the steady state are provided in Appendix D. In addition to steady-state parameters, as in Iacoviello and Neri (2010), we also fix the autocorrelation of the monetary policy shock to $\rho_s = 0.975$. The values of the calibrated parameters are reported in Appendix G. Overall, the number of estimated parameters is 35, and the calibrated parameters are 13.

The parameters that determine the rigidity of prices and wages through the adjustment costs *à la* Rotemberg (η_{π_1}, η_{π_2}, η_{w_1} and η_{w_2}) are unbounded and lack economic interpretability. We then map these parameters to the fractions of firms and unions that cannot reset prices and wages in an equivalent setting *à la* Calvo, see Richter and Throckmorton (2016). These fractions are respectively denoted by θ_{π_1}, θ_{π_2}, θ_{w_1} and θ_{w_2} (the complete optimization problems of retailers and labor unions are presented in Appendix A):

$$\eta_i = \frac{\theta_i(\epsilon_i - 1)}{(\beta\theta_i - 1)(\theta_i - 1)}, \qquad i = \pi_1, \pi_2, w_1, w_2.$$

The priors closely follow Smets and Wouters (2007). For the price and wage stickiness parameters, we specify the priors in terms of the Calvo-related parameter θ_i, $i \in$

[10] This normalization has been chosen by taking the average ratio of the chain price indexes of the two sectors, provided by U.S. Bureau of Economic Analysis, see Appendix C.

$\{\pi_1, \pi_2, w_1, w_2\}$, which can be linked to η_i according to:

$$\eta_i = \frac{\theta_i(\epsilon_i - 1)}{(\beta\theta_i - 1)(\theta_i - 1)}.$$

This provides a more direct interpretation of the parameter than the adjustment cost slope (η_i), and allows the use of standard priors. Priors and posteriors are summarized in Table 3. The priors reflect moderate consumption habits, moderate price and wage rigidities in the two sectors, substantial monetary policy inertia, moderate concern of the monetary authority for output stabilization, but a stronger concern for inflation. For all parameters, we impose symmetric priors across the two sectors and allow the likelihood to drive the sectoral differences found in the posterior density. For the autoregressive coefficients, the priors are loosely centered around 0.50.

7.3 Inference Strategy

The estimation is carried out using SMC already used in DSGE framework by Creal (2007, 2012) and Herbst and Schorfheide (2014, 2015). The SMC requires a likelihood tempering approach, which targets a sequence of tempered posterior densities $[p(\mathbf{y}_{1:T}|\theta)]^{\phi_n} p(\theta)$, with a tempering parameter $\phi_n \uparrow 1$, to gradually add to the prior the information from the likelihood, without incurring sample degeneracy and impoverishment problems. Moreover, the SMC algorithm can be parallelized on multiple processors, reducing computational time. In our estimation, we use a tempering schedule consisting of $N_\phi = 250$ bridge densities that determine the tempering schedule $\phi_n = \left(\frac{n-1}{N_\phi - 1}\right)$. The number of particles used in each bridge density is 80000, resulting in a total of 20 million likelihood evaluations. Following Durham and Geweke (2014), we assess convergence by running the algorithm multiple times and checking that the parameter estimates do not change.[11]

7.4 Estimation Results

Table 3 shows the posterior means and standard deviations of the parameters. The results suggest a high degree of habit formation, especially in the $\mathcal{S}_2$ sector, and a high degree of

[11] To avoid particle degeneracy the SMC requires a mutation step, that, according to Herbst and Schorfheide (2014) is a random walk with an adaptive covariance matrix based on the information contained in the previous draws and with an adaptive scaling factor that targets an acceptance probability of 25%.

stickiness in prices and wages in the $\mathcal{S}_1$ sector. Higher values of the indexation parameters in the general sector indicate significant levels of price and wage inertia. The small values of ν_1 and ν_2 are consistent with the large values of Frisch elasticity estimated in macro models. The capital adjustment and capacity utilization parameters point to higher degrees of real rigidity in $\mathcal{S}_1$. Taylor rule parameters indicate inertia in the policy rate and a higher weight associated with output stabilization than inflation control, in line with monetary policy evidence in the US. Finally, the posterior of the autoregressive parameters moves away from their diffuse priors, generally pointing to high degrees of persistence, particularly in the general sector.

Given the posterior estimates of parameters in Section 7, we run the MM-CKF up to 2021:Q4 and report the resulting filtered standardized shocks in Figure 7. As the figure shows, the shocks for the first quarter of the pandemic have a scale of orders of magnitude above the ordinary level defined in the range ± 3, similar to the results in Lenza and Primiceri (2022). For 2020:Q2 the filter detects large negative shocks to: (i) labor productivity in $\mathcal{S}_2$ ($\varepsilon_{z_2,t}$); (ii) labor supply in $\mathcal{S}_1$ ($\varepsilon_{\phi_1,t}$); (iii) demand in consumption of both goods ($\varepsilon_{\zeta,t}$); (iv) utility of consumption in $\mathcal{S}_2$ ($\varepsilon_{j,t}$); (v) labor productivity in $\mathcal{S}_1$ ($\varepsilon_{z_1,t}$). For 2020:Q3 the figure shows the partial recovery of the US economy. The filter detects a combination of large shocks: (i) a large positive rebound shock to intertemporal utility (ε_{ζ}); (ii) a rebound shock that reduces the disutility of working in $\mathcal{S}_1$ ($\varepsilon_{\phi_1,t}$); (iii) a large positive shock to labor productivity in $\mathcal{S}_1$ ($\varepsilon_{z_1,t}$). There are no large shocks in the contact intensive sector, in labor productivity in $\mathcal{S}_2$ ($\varepsilon_{z_2,t}$) and in the utility of consumption from $\mathcal{S}_2$ ($\varepsilon_{j,t}$). From 2020:Q4 to 2021:Q2 the real economy still suffers from the protracted Covid downturn. In 2020:Q4 we observe another contractionary shock to labor productivity in $\mathcal{S}_2$, a negative demand shock in both sectors, and a positive labor supply shock to the general sector, for quarters 2021:Q1 and 2021:Q2 we do not find large shocks. Finally, in 2021:Q3 and 2021:Q4 following the massive Covid vaccination campaign and the general reopenings in all sectors, we find large positive shocks in labor productivity in $\mathcal{S}_2$ for 2021:Q3 and 2021:Q4 and another reboud demand shock in the contact intensive sector $\mathcal{S}_2$ for 2021:Q3.

Similarly to Primiceri and Tambalotti (2020) and Lenza and Primiceri (2022), we consider only unanticipated shocks and their transmission. We think that assuming un-

Table 3: Estimation Results. Note: The table reports the parameter's name (Full Name) with the associate symbol (Symbol). The table also reports the prior shape (Prior), prior mean and standard deviation (Mean, St. Dev), and the posterior mean (Post. Mean) and standard deviation (Post. St. Dev) for the estimated parameters. $\mathcal{B}$ is the Beta distribution; $\mathcal{N}$ is the Normal distribution; $\mathcal{G}$ is the Gamma distribution; $\mathcal{IG}$ is the Inverse-Gamma distribution; $\mathcal{TN}$ is the Truncated Normal distribution on the interval $(0, 1)$.

Structural parameters					
Full Name	Symbol	Prior	(Mean, St. Dev.)	Posterior Mean	Posterior St. Dev
Habits $\mathcal{S}_1$	h_1	$\mathcal{B}$	(0.70, 0.10)	0.79	0.02
Habits $\mathcal{S}_2$	h_2	$\mathcal{B}$	(0.70, 0.10)	0.91	0.01
Price rigidity $\mathcal{S}_1$	θ_1	$\mathcal{B}$	(0.50, 0.10)	0.70	0.02
Price rigidity $\mathcal{S}_2$	θ_2	$\mathcal{B}$	(0.50, 0.10)	0.57	0.02
Inverse Frish el. $\mathcal{S}_1$	ν_1	$\mathcal{G}$	(0.50, 0.10)	0.25	0.05
Inverse Frish el. $\mathcal{S}_2$	ν_2	$\mathcal{G}$	(0.50, 0.10)	0.34	0.05
Taylor rule inertia	r_R	$\mathcal{B}$	(0.75, 0.10)	0.70	0.02
Taylor rule output reaction	r_Y	$\mathcal{N}$	(0.12, 0.05)	0.14	0.04
Taylor rule inflation reaction	r_π	$\mathcal{N}$	(2.00, 0.15)	1.99	0.02
Price indexation $\mathcal{S}_1$	ι_{π_1}	$\mathcal{B}$	(0.50, 0.15)	0.82	0.05
Price indexation $\mathcal{S}_2$	ι_{π_2}	$\mathcal{B}$	(0.50, 0.15)	0.82	0.05
Persistence Prod. $\mathcal{S}_1$	ρ_{z_1}	$\mathcal{B}$	(0.50, 0.20)	0.99	0.00
Persistence Prod. $\mathcal{S}_2$	ρ_{z_2}	$\mathcal{B}$	(0.50, 0,20)	0.18	0.07
Persistence Intratemp.	ρ_j	$\mathcal{B}$	(0.50, 0.20)	0.35	0.08
Persistence Lab. Supply $\mathcal{S}_1$	ρ_{ϕ_1}	$\mathcal{B}$	(0.50, 0.20)	0.73	0.03
Persistence Lab. Supply $\mathcal{S}_2$	ρ_{ϕ_2}	$\mathcal{B}$	(0.50, 0.20)	0.15	0.06
Persistence Intertemp.	ρ_ζ	$\mathcal{B}$	(0.50, 0.20)	0.67	0.03
Wage rigidity $\mathcal{S}_1$	θ_{w_1}	$\mathcal{B}$	(0.50, 0.10)	0.84	0.01
Wage rigidity $\mathcal{S}_2$	θ_{w_2}	$\mathcal{B}$	(0.50, 0.10)	0.68	0.02
Wage indexation $\mathcal{S}_1$	ι_{w_1}	$\mathcal{B}$	(0.50, 0.15)	0.88	0.05
Wage indexation $\mathcal{S}_2$	ι_{w_2}	$\mathcal{B}$	(0.50, 0.15)	0.77	0.11
Uiliz. adj.cost $\mathcal{S}_1$	$\eta_{u,1}$	$\mathcal{B}$	(0.50, 0.15)	0.92	0.04
Uiliz. adj.cost $\mathcal{S}_2$	$\eta_{u,2}$	$\mathcal{B}$	(0.50, 0.15)	0.22	0.06
Cap. adj.cost $\mathcal{S}_1$	η_{k_1}	$\mathcal{G}$	(10.00, 2.50)	13.38	0.96
Cap. adj.cost $\mathcal{S}_2$	η_{k_2}	$\mathcal{G}$	(10.00, 2.50)	12.10	2.38
Shock parameters					
Full Name	Symbol	Prior	(Mean, St. Dev.)	Posterior Mean	Posterior St. Dev
St. Dev. Prod. $\mathcal{S}_1$	$100 \times \sigma_{z_1}$	$\mathcal{IG}$	(1.00, ∞)	0.74	0.05
St. Dev. Temp. Mon. Policy	$100 \times \sigma_e$	$\mathcal{IG}$	(1.00, ∞)	0.29	0.02
St. Dev. Prod. $\mathcal{S}_2$	$100 \times \sigma_{z_2}$	$\mathcal{IG}$	(1.00, ∞)	1.39	0.12
St. Dev. Intratemp.	$100 \times \sigma_j$	$\mathcal{IG}$	(1.00, ∞)	10.98	0.76
St. Dev. Pers. Mon. Policy	$100 \times \sigma_s$	$\mathcal{IG}$	(1.00, ∞)	5.42	0.44
St. Dev. Lab. Supply $\mathcal{S}_1$	$100 \times \sigma_{\phi_1}$	$\mathcal{IG}$	(1.00, ∞)	6.14	0.34
St. Dev. Lab. Supply $\mathcal{S}_2$	$100 \times \sigma_{\phi_2}$	$\mathcal{IG}$	(1.00, ∞)	73.51	3.33
St. Dev. Pref.	$100 \times \sigma_\zeta$	$\mathcal{IG}$	(1.00, ∞)	2.97	0.25
Prepandemic Dis. Prob.	$1000 \times \psi_{pre}$	$\mathcal{TN}$	(0.01, 0.10)	0.57	0.23
Postpandemic Dis. Prob.	$100 \times \psi_{post}$	$\mathcal{TN}$	(99.00, 1.00)	99.10	0.45

expected rebound innovations is a reasonable choice. A rapid recovery like the one that actually occurred in 2020:Q3 can be considered unexpected given the information available in 2020:Q2, as also suggested by the forecasts presented in Primiceri and Tambalotti (2020) and Lenza and Primiceri (2022). In the baseline scenario of Primiceri and Tambalotti (2020), macroeconomic variables such as employment, consumption, and industrial

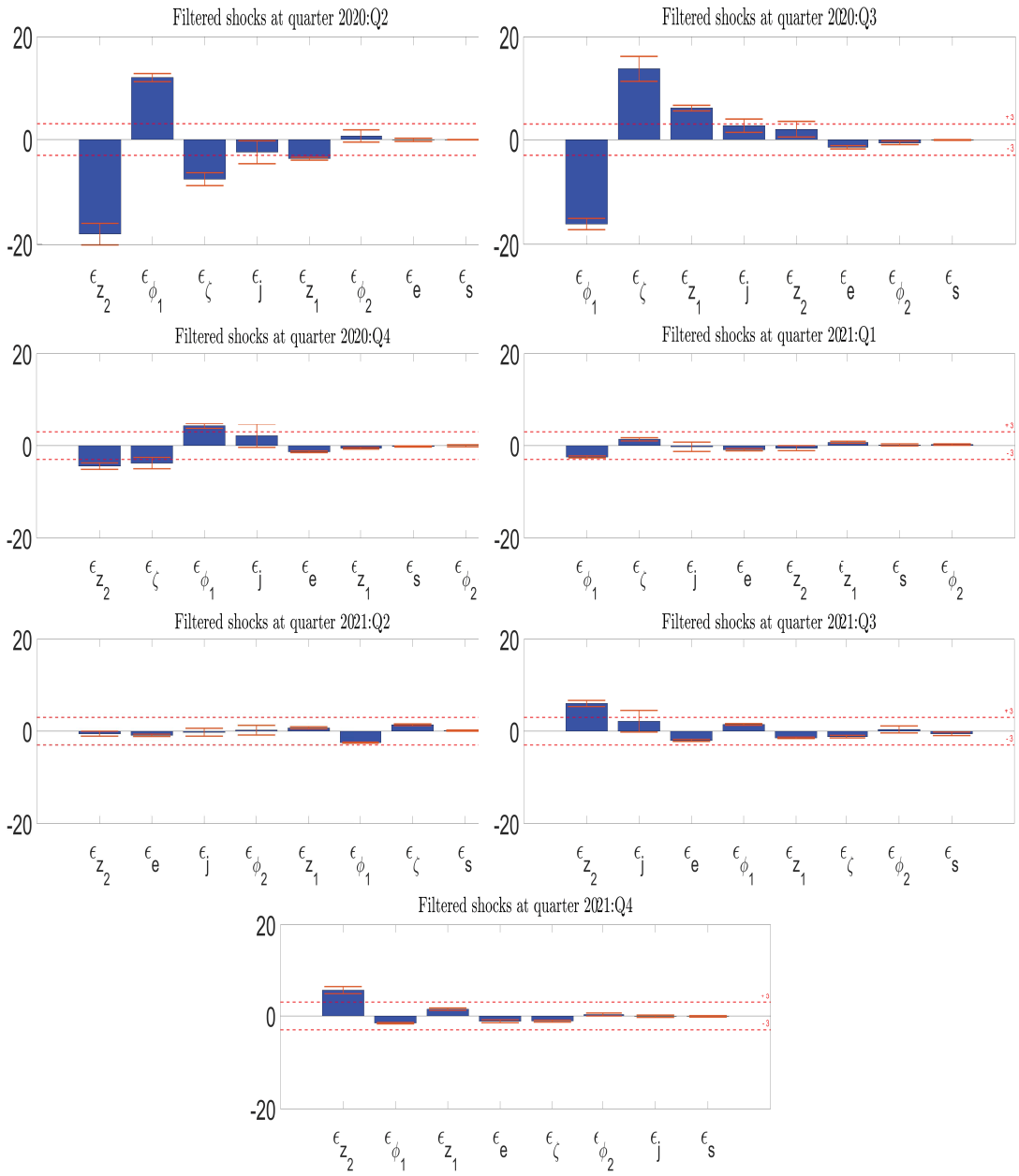

Figure 7: Filtered standardized shocks over time. Note: Bands represent one standard deviation resulting from parameter uncertainty. ε_{z_2}: labor productivity shock to $\mathcal{S}_2$. ε_{ϕ_1}: labor supply shock to $\mathcal{S}_1$. ε_ζ: demand shocks to both sectors. ε_j: demand shock to $\mathcal{S}_2$ services. ε_{z_1}: labor productivity shock to $\mathcal{S}_1$. ε_e: temporary monetary policy shock. ε_{ϕ_2}: labor supply shock to $\mathcal{S}_2$. ε_s: persistent monetary policy shock. The horizontal red dashed lines represent the values +3 and -3, as descriptive references for the reader.

production were expected to reach their trough in August 2020, rather than showing a large rebound. Also in Lenza and Primiceri (2022) the forecast of macroeconomic variables based on data until June 2020 shows a massive uncertainty.[12]

[12] Overall, after COVID-19 outbreak in 2020:Q2, the development of the Pandemic was highly uncertain depending on the different scenarios about reinfections, vaccinations, and new waves of contagion, and very different prospects for the recovery were put forward, as shown by various simulations obtained from using calibrated epidemiological models, see Eichenbaum et al. (2021), Bodenstein et al. (2020) and Kaplan et al. (2020).

7.5 Counterfactual and Robusness experiments

In our structural model, demand and supply shocks coexist, and their effects are jointly interdependent throughout the economy. We consider it reasonable that both production and preferences are affected by pandemic shocks. This point is also stressed by Guerrieri et al. (2020) with an emphasis on supply-side shocks that can be transmitted to the economy with demand-driven characteristics.[13]

To identify the contribution of each shock, without the potential spurious effect induced by demand and supply shock complementarities, we provide a counterfactual exercise. We evaluate the relative importance of the shocks by adding counterfactual variables ($\mathbf{y}_t^*$ and $\mathbf{x}_t^*$) in the state space presented in Section 3 (equations 12 and 13). These variables track the scenarios in which some shocks are switched off. The counterfactual state space representation is as follows:

$$\mathbf{y}_t^* = A + B\mathbf{x}_t^* + u_t, \qquad \mathbf{x}_t^* = f\left(x_{t-1}^S + R^*\tilde{\boldsymbol{\varepsilon}}_t\right). \tag{17}$$

For notational convenience state and control variables of the model are collapsed into the same vector $\mathbf{x}_t = \left[x_t^{C'}\, x_t^{S'}\right]'$ and the composite function $f(\cdot) = \left[g(h(\cdot))'\;\; h(\cdot)'\right]'$ combines $g(\cdot)$ and $h(\cdot)$ of equations (12). In Equation (17), the matrix R^* is constructed by equating to zero the columns of R in correspondence with the shocks set to zero, to test what happens when they do not occur. The object of interest in the counterfactual analysis is represented by the filtered counterfactual observables ($\mathbf{y}_t^*$).

Figure 8 reports the counterfactual experiment for 2020:Q2. The bars represent the predicted response of the variables corresponding to the indicated shock, with the others set to zero. The red dashed line represents the actual observations in the data, and the blue solid line represents the case where all shocks are set to zero. The interaction of shocks identified by our method is not negligible, and the sum of all individual contributions is not equal to the observed series. The 8% decline in production in $\mathcal{S}_1$ (ΔY_1) depends mainly on the large shocks to labor supply (ε_{ϕ_1}) and labor productivity (ε_{z_1}) in $\mathcal{S}_1$, and the decomposition of hours worked (Δn_1) is similar. On the contrary, the large negative

[13] It should be noted that the overall effect on the economy can be mixed, as both supply and demand shocks can be dampened or amplified by frictions and complementarities, as shown by Baqaee and Farhi (2021).

discount factor shock (ε_ζ) reduces aggregate consumption (ΔC) and increases aggregate investment (ΔI). The negative impact of the discount factor shock on consumption and investment is the same as in Smets and Wouters (2003), as this shock induces households to postpone consumption and therefore increase saving and capital investment. Since consumption and investment appear together in the resource constraint of the general sector (Equation 6), the overall effect of the discount factor shock on production is muted. Concerning sector $\mathcal{S}_2$, the decrease in production depends only on the intratemporal demand shock on consumption (ε_j) as production in this sector does not involve investment goods (Equation 7).[14] Looking at the dynamics of employment in $\mathcal{S}_2$ (Δn_2), the large reduction in productivity in $\mathcal{S}_2$ (ε_{z_2}) also has the effect of crowding out the use of capital in production in favor of labor, with a net negative effect due to the dominance of the intertemporal preference shock (ε_j). With respect to prices (π_1 and π_2), the decomposition shows counteracting effects. Indeed, the limited response of prices compared to the large fall in quantities is a stark feature of the COVID-19 economic disruption, suggesting the coexistence of supply and demand forces. For example, in $\mathcal{S}_1$, the negative labor supply shock (ε_{ϕ_1}) coexists with the negative discount factor (ε_ζ) shock which generates a milder deflation than we would observe if only demand shocks dominate.

Also in $\mathcal{S}_2$, inflation (π_2) has a similar decomposition; the graph shows that the negative labor productivity shock (ε_{z_2}) outweighs the negative sector-specific demand (ε_j) shock. This produces a mild positive inflation of around 1%. The bars illustrate that if the demand and supply shocks had occurred alone, considerably more extreme deflationary (-5.0%) or inflationary (+5.5%) outcomes would have occurred. Regarding wage inflation rates (ω_1 and ω_2), similar counteracting dynamics between demand and supply shocks emerge, with negative labor supply shocks providing a positive contribution to wage inflation in the related sector and negative demand shocks providing a negative contribution. Finally, supply shocks in the absence of demand shocks would have required a monetary tightening, as the central bank's price stability mandate would have outweighed the output stabilization goal. In general, as in Brinca et al. (2020) and Baqaee and Farhi (2021), among others, the estimates of the relative effects of supply and demand shocks suggest a combination of the two.

[14] The large shock to ε_j is not emphasized in Figure 7 because it is standardized. Given the large estimate of its standard deviation in Table 3, the non-standardized shock is large.

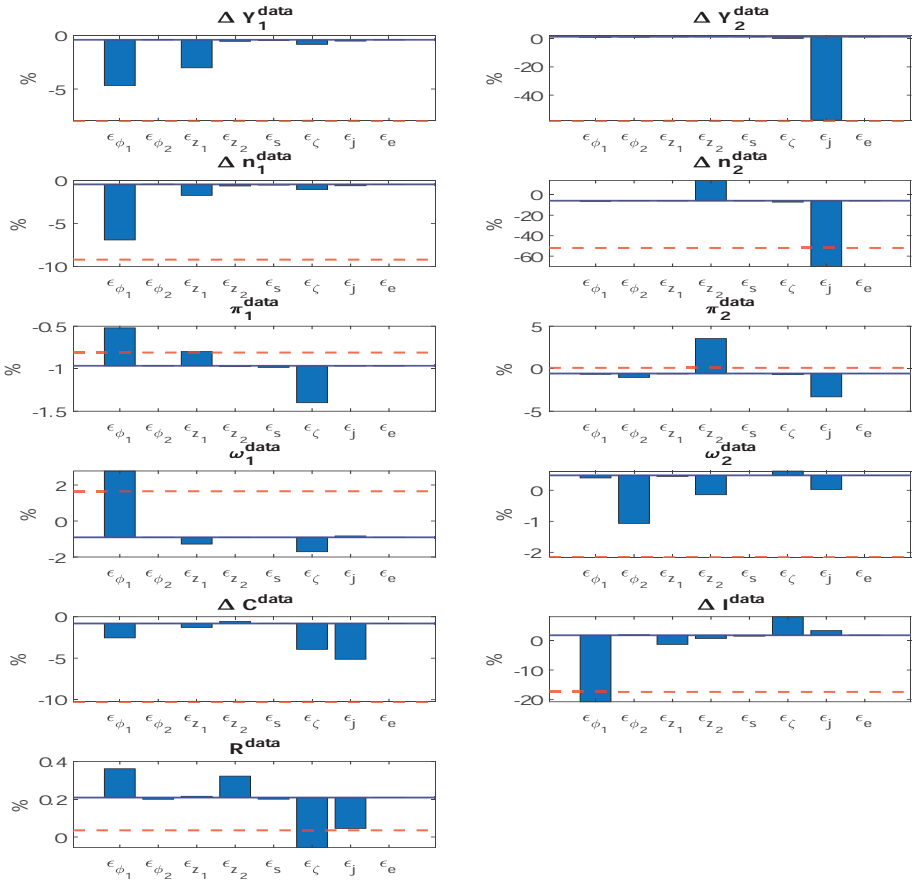

Figure 8: Contribution of individual shocks to the observed series for 2020:Q2. Note: Each bar corresponds to the counterfactual in which only the reported shock is switched on. The counterfactual simulations are obtained from the pruned state-space. The red dotted line represents the realized values. The blue solid line represents the counterfactual in which all shocks are switched off. Individual contributions do not add up to the observed series because of nonlinearity. The shocks are: demand shocks to both sectors (ε_ζ); labor supply shock to $\mathcal{S}_1$ (ε_{ϕ_1}); labor productivity shock to $\mathcal{S}_2$ (ε_{z_2}); labor productivity shock to $\mathcal{S}_1$ (ε_{z_1}); demand shock to $\mathcal{S}_2$ services (ε_j); labor supply shock to $\mathcal{S}_2$ (ε_{ϕ_2}); temporary monetary policy shock (ε_e) and persistent monetary policy shock (ε_s). The variables are: production in $\mathcal{S}_1$ (ΔY_1^{data}); production in $\mathcal{S}_2$ (ΔY_2^{data}); hours in $\mathcal{S}_1$ (Δn_1^{data}); hours in $\mathcal{S}_2$ (Δn_2^{data}); inflation in $\mathcal{S}_1$ (π_1^{data}); inflation in $\mathcal{S}_2$ (π_2^{data}); wage inflation in $\mathcal{S}_1$ (ω_1^{data}); wage inflation in $\mathcal{S}_2$ (ω_2^{data}); aggregate consumption (ΔC^{data}); aggregate investment (ΔI^{data}) and the interest rate (R^{data}).

7.6 Robustness

We now provide a robustness exercise. Given that a large part of the complications arise from inference on parameters with pandemic data, a more naive approach would be to stop the estimation before 2020 and identify the large shocks occurring in 2020 using the previously estimated parameters. This approach has been applied in the VAR setting by Brinca et al. (2020). The drawback of this strategy is that it implies treating the pandemic observations as missing and neglecting their information content for the model parameters, even if these outliers will remain in the sample forever. We estimate the parameters of the model in a sample that ends before the pandemic (2019:Q4) and run the filter. These parameter estimates are reported in Appendix E. Figure 9 shows the comparison of this naive approach with the one proposed in the paper. The model parameters remain stable when pandemic quarters are excluded. Consequently, in Figure 9 the filtered shocks do not change much using this strategy (*No pandemic* column) from the baseline estimation that applies our method (*Baseline Sample* column). It is visible, though, that the identified shocks from the pre-pandemic estimation display larger uncertainty. To show that our modelization of large shocks is important, we estimate the model on the full sample without imposing non-Gaussian shocks. These parameter estimates are also reported in Appendix E. In this case, the parameter estimates change substantially given the large influence of the pandemic quarters. Consequently, in Figure 9 also the filtered shocks change considerably using this strategy (*No LS* column) from the baseline estimation (*Baseline Sample* column).

8 Conclusion

This paper builds and estimates a two-sector medium-scale new Keynesian model to study the type, magnitude, and direction of economic shocks during the pandemic. The model includes the standard real and nominal frictions used in the empirical literature and allows heterogeneous exposure to the COVID-19 pandemic across sectors.

We solve the model nonlinearly and, to make inferences, we propose a new nonlinear, non-Gaussian filter designed to handle and identify large shocks. Monte Carlo experiments show that our filter can correctly identify the source and time location of shocks and outperform particle filters with a massively reduced running time, allowing us to estimate

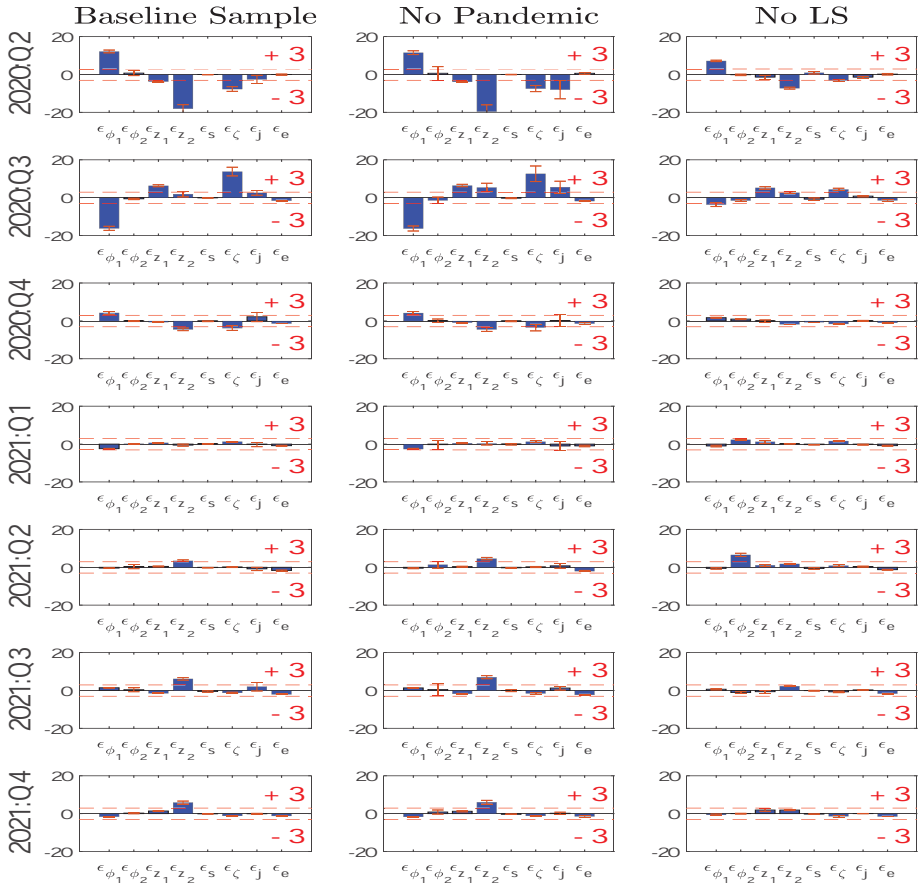

Figure 9: Filtered standardized shocks during and after the pandemic. Note: The panels in the left column refer to the Baseline estimation, the ones in the middle refer to the No-Pandemic estimation, while the ones in the right column refer to the No Large shocks specification. The bands represent one standard deviation resulting from parameter uncertainty. ε_{z_2}: labor productivity shock to $\mathcal{S}_2$. ε_{ϕ_1}: labor supply shock to $\mathcal{S}_1$. ε_{ζ}: demand shocks to both sectors. ε_j: demand shock to $\mathcal{S}_2$ services. ε_{z_1}: labor productivity shock to $\mathcal{S}_1$. ε_e: temporary monetary policy shock. ε_{ϕ_2}: labor supply shock to $\mathcal{S}_2$. ε_s: persistent monetary policy shock. The horizontal red dashed lines represent the values +3 and -3, as descriptive references for the reader.

the model efficiently using the Sequential Monte Carlo sampler recently proposed by Herbst and Schorfheide (2014).

The empirical results indicate that economic disruption is caused by a combination of demand and supply shocks rather than supply or demand shocks alone. In 2020:Q2, we identify a large negative shock in the demand for goods produced by the general sector, together with a large negative shock in the demand for contact-intensive products. On the supply side, we detected a large labor supply shock in the general sector and a large labor productivity shock in the pandemic-sensitive sector.

We analyze the effects of these shocks by performing a set of counterfactual experi-

ments. We find that if only demand and supply shocks were in action, the responses of the model variables would have differed substantially from what is observed in the data. In the robustness part, we also show that our modellization of large shocks allows us to estimate model parameters that are stable compared to estimation on prepandemic data and that the absence of this modellization would lead to unstable results.

References

Abo-Zaid, S. and Xuguang, S. S. (2020). Health Shocks in a General Equilibrium Model. Available at ssrn: https://ssrn.com/abstract=3611404.

Adjemian, S., Bastani, H., Juillard, M., Karamé, F., Mihoubi, F., Mutschler, W., Pfeifer, J., Ratto, M., Rion, N., and Villemot, S. (2022). Dynare: Reference Manual Version 5. Dynare Working Papers 72, CEPREMAP.

Alspach, D. and Sorenson, H. (1972). Nonlinear Bayesian Estimation Using Gaussian Sum Approximations. *IEEE transactions on automatic control*, 17:439–448.

Amisano, G. and Tristani, O. (2010). Euro Area Inflation Persistence in an Estimated Nonlinear DSGE model. *Journal of Economic Dynamics and Control*, 34:1837–1858.

Amisano, G. and Tristani, O. (2011). Exact Likelihood Computation for Nonlinear DSGE Models with Heteroskedastic Innovations. *Journal of Economic Dynamics and Control*, 35:2167–2185.

An, S. and Schorfheide, F. (2007). Bayesian Analysis of DSGE Models. *Econometric reviews*, 26:113–172.

Andreasen, M. M. (2011). Non-Linear DSGE Models and the Optimized Central Difference Particle Filter. *Journal of Economic Dynamics and Control*, 35:1671–1695.

Andreasen, M. M. (2012a). An Estimated DSGE Model: Explaining Variation in Nominal Term Premia, Real Term Premia, and Inflation Risk Premia. *European Economic Review*, 56:1656–1674.

Andreasen, M. M. (2012b). On the Effects of Rare Disasters and Uncertainty Shocks for Risk Premia in Non-Linear DSGE Models. *Review of Economic Dynamics*, 15:295–316.

Andreasen, M. M. (2013). Non-linear DSGE Models and the Central Difference Kalman Filter. *Journal of Applied Econometrics*, 28:929–955.

Arasaratnam, I. and Haykin, S. (2009). Cubature Kalman Filters. *IEEE Transactions on Automatic Control*, 54:1254–1269.

Arasaratnam, I., Haykin, S., and Elliott, R. J. (2007). Discrete-time Nonlinear Filtering Algorithms using Gauss–Hermite Quadrature. *Proceedings of the IEEE*, 95:953–977.

Aruoba, S. B., Cuba-Borda, P., Higa-Flores, K., Schorfheide, F., and Villalvazo, S. (2021). Piecewise-Linear Approximations and Filtering for DSGE Models with Occasionally Binding Constraints. *Review of Economic Dynamics*, 41:96–120.

Baqaee, D. R. and Farhi, E. (2021). Supply and Demand in Disaggregated Keynesian Economies with an Application to the Covid-19 Crisis. NBER Working Paper N. 27152.

Bengtsson, T., Bickel, P., Li, B., et al. (2008). Curse-of-Dimensionality Revisited: Collapse of the Particle Filter in Very Large Scale Systems. In *Probability and statistics: Essays in honor of David A. Freedman*, pages 316–334. Institute of Mathematical Statistics.

Benigno, G., Foerster, A., Otrok, C., and Rebucci, A. (2020). Estimating Macroeconomic Models of Financial Crises: An Endogenous Regime-Switching Approach. NBER Working Paper N. 26935.

Bernanke, B. S., Gertler, M., and Gilchrist, S. (1999). The Financial Accelerator in a Quantitative Business Cycle Framework. *Handbook of macroeconomics*, 1:1341–1393.

Binning, A. and Maih, J. (2015). Sigma Point Filters for Dynamic Nonlinear Regime Switching Models. Norges Bank Working Paper N. 10-2015.

Bodenstein, M., Corsetti, G., and Guerrieri, L. (2020). Social Distancing and Supply Disruptions in a Pandemic. CEPR Discussion Paper N. DP14629.

Brinca, P., Duarte, J. B., and Faria-e Castro, M. (2020). Measuring Sectoral Supply and Demand Shocks During COVID-19. Federal Reserve Board St.Louis Working paper 2020-011.

Cai, M., Del Negro, M., Herbst, E., Matlin, E., Sarfati, R., and Schorfheide, F. (2021). Online Estimation of DSGE Models. *The Econometrics Journal*, 24:33–58.

Cardani, R., Croitorov, O., Giovannini, M., Pfeiffer, P., Ratto, M., and Vogel, L. (2022). The Euro Area's Pandemic Recession: A DSGE-based Interpretation. *Journal of Economic Dynamics and Control*, 143:104512.

Carriero, A., Clark, T. E., Marcellino, M. G., and Mertens, E. (2022). Addressing COVID-19 Outliers in BVARs with Stochastic Volatility. *The Review of Economics and Statistics*, 11:1–38.

Chib, S. and Ramamurthy, S. (2014). DSGE Models with Student-t Errors. *Econometric Reviews*, 33:152–171.

Creal, D. D. (2007). Sequential Monte Carlo Samplers for Bayesian DSGE Models. *Manuscript, University Chicago Booth*, pages 245–296.

Creal, D. D. (2012). A Survey of Sequential Monte Carlo Methods for Economics and Finance. *Econometric reviews*, 31:245–296.

Creal, D. D. (2017). A Class of Non-Gaussian State Space Models With Exact Likelihood Inference. *Journal of Business & Economic Statistics*, 35:585–597.

Cúrdia, V., Del Negro, M., and Greenwald, D. L. (2014). Rare Shocks, Great Recessions. *Journal of Applied Econometrics*, 29:1031–1052.

Del Negro, M. and Schorfheide, F. (2008). Forming Priors for DSGE Models (and How it Affects the Assessment of Nominal Rigidities). *Journal of Monetary Economics*, 55:1191–1208.

del Rio-Chanona, R. M., Mealy, P., Pichler, A., Lafond, F., and Farmer, J. D. (2020). Supply and Demand Shocks in the COVID-19 Pandemic: An Industry and Occupation Perspective. *Oxford Review of Economic Policy*, 36:94–137.

Dewachter, H. and Wouters, R. (2014). Endogenous Risk in a DSGE Model with Capital-Constrained Financial Intermediaries. *Journal of Economic Dynamics and control*, 43:241–268.

Durbin, J. and Koopman, S. J. (2012). *Time Series Analysis by State Space Methods*. Oxford University Press.

Durham, G. and Geweke, J. (2014). Adaptive Sequential Posterior Simulators for Massively Parallel Computing Environments. In *Bayesian model comparison*. Emerald Group Publishing Limited.

Eichenbaum, M. S., Rebelo, S., and Trabandt, M. (2021). The Macroeconomics of Epidemics. *The Review of Financial Studies*, 34:5149–5187.

Eichenbaum, M. S., Rebelo, S., and Trabandt, M. (2022). Epidemics in the Neoclassical and New Keynesian Models. *Journal of Economic Dynamics and Controln*, 140:1–19.

Faria-e Castro, M. (2021). Fiscal Policy During a Pandemic. *Journal of Economic Dynamics & Control*, 125:104–135.

Faubel, F., McDonough, J., and Klakow, D. (2009). The Split and Merge Unscented Gaussian Mixture Filter. *IEEE Signal Processing Letters*, 16:786–789.

Fernández-Villaverde, J., Guerrón-Quintana, P., Rubio-Ramírez, J. F., and Uribe, M. (2011). Risk Matters: The Real Effects of Volatility Shocks. *American Economic Review*, 101:2530–2561.

Fernández-Villaverde, J. and Jones, C. I. (2022). Estimating and Simulating a SIRD Model of COVID-19 for Many Countries, States, and Cities. *Journal of Economic Dynamics and Control*, 140:104–130.

Fernández-Villaverde, J. and Rubio-Ramírez, J. F. (2007). Estimating Macroeconomic Models: A Likelihood Approach. *The Review of Economic Studies*, 74:1059–1087.

Ferroni, F., Fisher, J. D., and Melosi, L. (2022). Unusual Shocks in Our Usual Models. FRB of Chicago Working Paper No 2022-39.

Flury, T. and Shephard, N. (2011). Bayesian Inference Based Only on Simulated Likelihood: Particle Filter Analysis of Dynamic Economic Models. *Econometric Theory*, 27:933–956.

Fornaro, L. and Wolf, M. (2020). Covid-19 Coronavirus and Macroeconomic Policy. CEPR Discussion Paper N. DP14529.

Fornaro, L. and Wolf, M. (2023). The Scars of Supply Shocks: Implication for Monetary Policy. *Journal of Monetary Economics, Forthcoming*.

Gordon, N. J., Salmond, D. J., and Smith, A. F. (1993). Novel Approach to Nonlinear/Non-Gaussian Bayesian State Estimation. In *IEE proceedings F (radar and signal processing)*, volume 140, pages 107–113.

Gourio, F. (2012). Disaster Risk and Business Cycles. *American Economic Review*, 102:2734–2766.

Guerrieri, V., Lorenzoni, G., Straub, L., and Werning, I. (2020). Macroeconomic Implications of COVID-19: Can Negative Supply Shocks Cause Demand Shortages? NBER Working Paper N. 26918.

Herbst, E. and Schorfheide, F. (2014). Sequential Monte Carlo Sampling for DSGE Models. *Journal of Applied Econometrics*, 29:1073–1098.

Herbst, E. P. and Schorfheide, F. (2015). *Bayesian Estimation of DSGE Models*. Princeton University Press.

Iacoviello, M. and Neri, S. (2010). Housing Market Spillovers: Evidence from an Estimated DSGE Model. *American Economic Journal: Macroeconomics*, 2:125–164.

Ito, K. and Xiong, K. (2000). Gaussian Filters for Nonlinear Filtering Problems. *IEEE Transactions on Automatic Control*, 45:910–927.

Ivashchenko, S. (2014). DSGE Model Estimation on the Basis of Second-Order Approximation. *Computational Economics*, 43:71–82.

Jia, B., Xin, M., and Cheng, Y. (2013). High-Degree Cubature Kalman Filter. *Automatica*, 49:510–518.

Kaplan, G., Moll, B., and Violante, G. L. (2020). The Great Lockdown and the Big Stimulus: Tracing the Pandemic Possibility Frontier for the US. NBER Working Paper N. 27794.

Kollmann, R. (2015). Tractable Latent State Filtering for Non-linear DSGE Models Using a Second-Order Approximation and Pruning. *Computational Economics*, 45:239–260.

Kotecha, J. H. and Djuric, P. M. (2003). Gaussian-Sum Particle Filtering. *IEEE Transactions on Signal Processing*, 51:2602–2612.

Lenza, M. and Primiceri, G. E. (2022). How to Estimate a VAR after March 2020. *Journal of Applied Econometrics*, 37:688–699.

Leong, P. H., Arulampalam, S., Lamahewa, T. A., and Abhayapala, T. D. (2013). A Gaussian-Sum Based Cubature Kalman Filter for Bearings-Only Tracking. *IEEE Transactions on Aerospace and Electronic Systems*, 49:1161–1176.

Levintal, O. (2017). Fifth-Order Perturbation Solution to DSGE Models. *Journal of Economic Dynamics and Control*, 80:1–16.

Liu, J. S. and Chen, R. (1998). Sequential Monte Carlo Methods for Dynamic Systems. *Journal of the American Statistical Association*, 93:1032–1044.

Noh, S. (2020). Posterior Inference on Parameters in a Nonlinear DSGE Model via Gaussian-Based Filters. *Computational Economics*, 56:795–841.

Pei, H. L., Arulampalam, S., Lamahewa, A. T., and Abhayapala, D. T. (2013). A Gaussian-Sum Based Cubature Kalman Filter for Bearings-Only Tracking. *IEEE Transactions on Aerospace and Electronic Systems*, 49:1161–1176.

Pei, H. L., Arulampalam, S., Lamahewa, A. T., and Abhayapala, D. T. (2014). Gaussian-Sum Cubature Kalman Filter with Improved Robustness for Bearings-only Tracking. *IEEE Signal Processing Letters*, 21:513–517.

Pitt, M. K. and Shephard, N. (1999). Filtering Via Simulation: Auxiliary Particle Filters. *Journal of the American Statistical Association*, 94:590–599.

Primiceri, G. E. and Tambalotti, A. (2020). Macroeconomic Forecasting in the Time of COVID-19. *Manuscript, Northwestern University*, pages 1–23.

Richter, A. W. and Throckmorton, N. A. (2016). Is Rotemberg Pricing Justified by Macro Data? *Economics Letters*, 149:44–48.

Särkkä, S. (2013). *Bayesian Filtering and Smoothing*. Cambridge University Press.

Schmitt-Grohé, S. and Uribe, M. (2004). Solving Dynamic General Equilibrium Models Using a Second-Order Approximation to the Policy Function. *Journal of economic dynamics and control*, 28:755–775.

Smets, F. and Wouters, R. (2003). An Estimated Dynamic Stochastic General Equilibrium Model of the Euro Area. *Journal of the European Economic Association*, 1:1123–1175.

Smets, F. and Wouters, R. (2007). Shocks and Frictions in US Business Cycles: A Bayesian DSGE Approach. *American Economic Review*, 97:586–606.

Sorenson, H. W. and Alspach, D. L. (1971). Recursive Bayesian Estimation using Gaussian-Sums. *Automatica*, 7:465–479.

Wan, E. A. and Van Der Merwe, R. (2000). The Unscented Kalman Filter for Nonlinear Estimation. *Proceedings of the IEEE 2000 Adaptive Systems for Signal Processing, Communications, and Control Symposium*, 1:153–158.

Woodford, M. (2020). Effective Demand Failures and the Limits of Monetary Stabilization Policy. NBER Working Paper N. 27768.

A The Model Equations

Households

The functional forms of the investment and capacity utilization costs appearing in the household's budget constraint (eq. 2) are the following:

$$\Psi_{k_{1,t}} = \frac{\eta_{k_1}}{2}\left(\frac{k_{1,t}}{k_{1,t-1}} - 1\right)^2 k_{1,t-1}, \quad \Psi_{k_2,t} = \frac{\eta_{k_2}}{2}\left(\frac{k_{2,t}}{k_{2,t-1}} - 1\right)^2 k_{2,t-1},$$

$$\Psi_{u_1,t} = \left(\frac{1}{\beta} - (1-\delta_{k_1})\right)\left[\frac{\left(\frac{\eta_{u_1}}{1-\eta_{u_1}}\right)}{2} + \frac{\left(\frac{\eta_{u_1}}{1-\eta_{u_1}}\right)}{2}u_{k_1,t}^2 + u_{k_1,t}\left(1 - \frac{\eta_{u_1}}{1-\eta_{u_1}}\right) - 1\right],$$

$$\Psi_{u_2,t} = \left(\frac{1}{\beta} - (1-\delta_{k_2})\right)\left[\frac{\left(\frac{\eta_{u_2}}{1-\eta_{u_2}}\right)}{2} + \frac{\left(\frac{\eta_{u_2}}{1-\eta_{u_2}}\right)}{2}u_{k_2,t}^2 + \left(1 - \frac{\eta_{u_2}}{1-\eta_{u_2}}\right)u_{k_2,t} - 1\right].$$

The term Ψ_t in the household's budget constraint (eq. 2) is then given by:

$$\Psi_t = \Psi_{k_1,t} + p_{2,t}\Psi_{k_2,t} + \Psi_{u_1,t}k_{1,t-1} + p_{2,t}\Psi_{u_2,t}k_{2,t-1}.$$

The household's optimization leads to the following first-order conditions:

- Euler equation:

$$u_{c_1,t} = \beta R_t \mathbb{E}_t\left(\frac{u_{c_1,t+1}}{\pi_{1,t+1}}\right). \tag{18}$$

- Intratemporal consumption condition:

$$\frac{u_{c_2,t}}{p_{2,t}} = u_{c_1,t}. \tag{19}$$

- Labor supply to $\mathcal{S}_1$ and $\mathcal{S}_2$:

$$a_{\zeta,t}\phi_{1,t}n_{1,t}^{\nu_1} = \frac{w_{1,t}u_{c_1,t}}{X_{w_1,t}}, \quad a_{\zeta,t}\phi_{2,t}n_{2,t}^{\nu_2} = \frac{w_{2,t}u_{c_2,t}}{X_{w_2,t}}. \tag{20}$$

- Capital supply to $\mathcal{S}_1$:

$$\begin{aligned} &u_{c_1,t}\left[1 + \eta_{k_1}\left(\frac{k_{1,t}}{k_{1,t-1}} - 1\right)\right] \\ &\quad = \beta\mathbb{E}_t u_{c_1,t+1}\left[1 - \delta_{k_1} + r_{k_1,t+1}u_{k_1,t+1} + \frac{\eta_{k_1}}{2}\left(\frac{k_{1,t+1}^2}{k_{1,t}^2} - 1\right)\right]. \end{aligned} \tag{21}$$

- Capital supply to $\mathcal{S}_2$:

$$\begin{aligned} & p_{2,t}u_{c_1,t}\left[1+\eta_{k_2}\left(\frac{k_{2,t}}{k_{2,t-1}}-1\right)\right] \\ & \quad = \beta\mathbb{E}_t p_{2,t+1}u_{c_1,t+1}\left[1-\delta_{k2}+r_{k_2,t+1}u_{k_2,t+1}+\frac{\eta_{k_2}}{2}\left(\frac{k_{2,t+1}^2}{k_{2,t}^2}-1\right)\right]. \end{aligned} \tag{22}$$

- Capacity utilization in $\mathcal{S}_1$ condition:

$$\frac{r_{k_1,t}}{\frac{1}{\beta}-(1-\delta_{k_1})} = 1-\frac{\eta_{u,1}}{1-\eta_{u,1}}+\frac{\eta_{u,1}}{1-\eta_{u,1}}\,u_{k_1,t}. \tag{23}$$

- Capacity utilization in $\mathcal{S}_2$ condition:

$$\frac{r_{k_2,t}}{\frac{1}{\beta}-(1-\delta_{k_2})} = 1-\frac{\eta_{u,2}}{1-\eta_{u,2}}+\left(\frac{\eta_{u,2}}{1-\eta_{u,2}}\right)u_{k_2,t}. \tag{24}$$

where the marginal utilities of consumption are defined by:

$$u_{c_1,t} = \frac{1-h_1}{1-\beta h_1}\left(\frac{a_{\zeta,t}}{c_{1,t}-h_1c_{1,t-1}}-\mathbb{E}_t\frac{h_1\beta a_{\zeta,t+1}}{c_{1,t+1}-h_1c_{1,t}}\right),$$

$$u_{c_2,t} = \frac{1-h_2}{1-\beta h_2}\left[\frac{a_{\zeta,t}a_{j,t}}{c_{2,t}-h_2c_{2,t-1}}-\mathbb{E}_t\left(\frac{h_2\beta a_{\zeta,t+1}a_{j,t+1}}{c_{2,t+1}-h_2c_{2,t}}\right)\right].$$

Eq. (18) is the Euler equation with respect to the first good, eq. (19) is the intratemporal condition between the two goods, eqs. (20) are the labor supply conditions, (21) and (22) pin down capital supply, while (23) and (24) are the capacity utilization conditions.

Wholesale Firms

First-order conditions of the wholesale firms consist in the following equations:

- Labor demand by $\mathcal{S}_1$ and $\mathcal{S}_2$:

$$\frac{(1-\alpha_1)\,Y_{1,t}}{X_{1,t}} = w_{1,t}n_{1,t}, \qquad \frac{(1-\alpha_2)\,Y_{2,t}}{X_{2,t}} = w_{2,t}n_{2,t}. \tag{25}$$

- Capital demand by $\mathcal{S}_1$ and $\mathcal{S}_2$:

$$\frac{\alpha_1 Y_{1,t}}{X_{1,t}} = r_{k_1,t}u_{k_1,t}\,k_{1,t-1}, \qquad \frac{\alpha_2 Y_{2,t}}{X_{2,t}} = r_{k_2,t}u_{k_2,t}\,k_{2,t-1}. \tag{26}$$

Eqs. (25) are the labor demand conditions, while eqs. (26) govern capital demand.

Retail Firms

Retailers face quadratic adjustment costs à la Rotemberg in changes in retail prices ($P_{1,t}(j)$ and $P_{2,t}(j)$). Adjustment costs depend on last quarter's inflation, with weights given by the indexation parameters ι_{π_1} and ι_{π_2}. The retail firm problem is therefore (for sectors $i = 1, 2$) to set $P_{i,t}(j)$ to maximize:

$$\mathbb{E}_0 \sum_{t=0}^{\infty} \beta^t \left\{ \frac{u_{c_1,t}}{u_{c_1,0}} \left[\frac{P_{i,t}(j)}{P_{i,t}} Y_{i,t}(j) - \frac{1}{X_{i,t}} Y_{i,t}(j) - \frac{\eta_i}{2} \left(\frac{P_{i,t}(j)}{P_{i,t-1}(j)} - \pi_{i,t-1}^{\iota_{\pi_i}} \right)^2 Y_{i,t} \right] \right\}, \qquad (27)$$

subject to:

$$Y_{i,t}(j) = \left(\frac{P_{i,t}(j)}{P_{i,t}} \right)^{-\epsilon_{\pi_i}} Y_{i,t}.$$

This optimization problem shows that deviations of the prices of individual varieties $\left(\frac{P_{i,t}(j)}{P_{i,t-1}(j)}\right)$ from the aggregate inflation $(\pi_{i,t-1}^{\iota_{\pi_i}})$ are penalized, depending on the rigidity parameters η_i. Moreover, as visible from eq. (27), at each time t the profits of retailers are weighted by the stochastic discount rate $\left(\beta^t \frac{u_{c_1,t}}{u_{c_1,0}}\right)$, which depends on the marginal utility of consumption at time t. In the case of fully flexible prices ($\eta_\pi = 0$), the markup is set at its steady-state value $X_i = \frac{\epsilon_{\pi_i}}{\epsilon_{\pi_i} - 1}$. The price-setting problem of retail firms gives the two Phillips curves:

- Price Phillips curve for $\mathcal{S}_1$:

$$1 - \pi_{1,t}\eta_{\pi_1} \left(\pi_{1,t} - \pi_{1,t-1}^{\iota_{\pi_1}} \right) + \beta \eta_{\pi_1} \mathbb{E}_t \left[\pi_{1,t+1} \frac{u_{c_1,t+1}}{u_{c_1,t}} \left(\pi_{1,t+1} - \pi_{1,t}^{\iota_{\pi_1}} \right) \frac{Y_{1,t+1}}{Y_{1,t}} \right]$$
$$= \left(1 - \frac{1}{X_{1,t}} \right) \epsilon_{\pi_1}.$$

- Price Phillips curve for $\mathcal{S}_2$:

$$1 - \pi_{2,t}\eta_{\pi_2} \left(\pi_{2,t} - \pi_{2,t-1}^{\iota_{\pi_2}} \right) + \beta \eta_{\pi_2} \mathbb{E}_t \left[\pi_{2,t+1} \frac{u_{c_1,t+1}}{u_{c_1,t}} \left(\pi_{2,t+1} - \pi_{2,t}^{\iota_{\pi_2}} \right) \frac{Y_{2,t+1}}{Y_{2,t}} \right]$$
$$= \left(1 - \frac{1}{X_{2,t}} \right) \epsilon_{\pi_2}.$$

Retailers' profits are finally equal to:

$$\Pi_{r_1,t} = \left(1 - \frac{1}{X_{1,t}}\right) Y_{1,t} - \frac{\eta_{\pi_1}}{2} \left(\pi_{1,t} - \pi_{1,t-1}^{\iota_{\pi_1}}\right)^2 Y_{1,t},$$

$$\Pi_{r_2,t} = \left(1 - \frac{1}{X_{2,t}}\right) Y_{2,t} - \frac{\eta_{\pi_2}}{2} \left(\pi_{2,t} - \pi_{2,t-1}^{\iota_{\pi_2}}\right)^2 Y_{2,t}.$$

Unions

Unions buy homogeneous labor services from households and differentiate them at no cost. Differentiated labor varieties are then aggregated back into CES aggregates by labor packers in homogeneous compounds, which are sold to the wholesale firm. The enforcement of wage rigidities through labor unions is in line with Smets and Wouters (2007) and Iacoviello and Neri (2010), among others, and similarly to final goods price, it results from the presence of adjustment costs à la Rotemberg (with indexation parameters ι_{w_1} and ι_{w_2}). Labor unions face the demand schedule $n_{i,t}(h) = \left(\frac{W_{i,t}(h)}{W_{i,t}}\right)^{-\epsilon_{w_i}} n_{i,t}$, $i = 1, 2$, and maximize:

$$\mathbb{E}_0 \sum_{t=0}^{\infty} \beta^t \left\{ \frac{u_{c_1,t}}{u_{c_1,0}} \left[\frac{W_{i,t}(h)}{P_{i,t}} n_{i,t}(h) - \frac{\eta_{w_i}}{2} \left(\frac{W_{i,t}(h)}{W_{i,t-1}(h)} - \pi_{i,t-1}^{\iota_{w_i}} \right)^2 \frac{W_{i,t}}{P_{i,t}} \right] - \frac{a_{\zeta,t} \phi_{i,t} n_{i,t}(h)^{1+\nu_i}}{1+\nu_i} \right\}.$$

The maximization of labor unions' profits gives the two wage Phillips curves:

- Wage Phillips curve for $\mathcal{S}_1$:

$$\eta_{w_1} \omega_{1,t} \left(\omega_{1,t} - \pi_{1,t-1}^{\iota_{w_1}}\right) = \beta \eta_{w_1} \mathbb{E}_t \frac{u_{c_1,t+1}}{u_{c_1,t}} \left(\omega_{1,t+1} - \pi_{1,t}^{\iota_{w_1}}\right) \frac{\omega_{1,t+1}^2}{\pi_{1,t+1}} + (1 - \epsilon_{w_1})\, n_{1,t} + \epsilon_{w_1} \left(\frac{\phi_{1,t}, n_{1,t}^{1+\nu_1}}{w_{1,t} u_{c_1,t}} \right). \tag{28}$$

- Wage Phillips curve for $\mathcal{S}_2$:

$$\eta_{w_2} \omega_{2,t} \left(\omega_{2,t} - \pi_{2,t-1}^{\iota_{w_2}}\right) = \beta \eta_{w_2} \mathbb{E}_t \frac{u_{c_1,t+1}}{u_{c_1,t}} \left(\omega_{2,t+1} - \pi_{2,t}^{\iota_{w_2}}\right) \frac{\omega_{2,t+1}^2}{\pi_{2,t+1}} + (1 - \epsilon_{w_2})\, n_{2,t} + \epsilon_{w_2} \left(\frac{\phi_{2,t} {n_{2,t}}^{1+\nu_2}}{p_{2,t} w_{2,t} u_{c_1,t}} \right). \tag{29}$$

Above, $\omega_{1,t}$ and $\omega_{2,t}$ are nominal wage inflation, namely $\omega_{i,t} = \frac{W_{i,t}}{W_{i,t-1}} = \frac{P_{i,t}w_{i,t}}{P_{i,t-1}w_{i,t-1}} = \pi_{i,t}\frac{w_{i,t}}{w_{i,t-1}}$. Unions' profits are finally given by margins minus adjustment costs:

$$\Pi_{u_1,t} = \left(1 - \frac{1}{X_{w_1,t}}\right) w_{1,t}\, n_{1,t} - \frac{\eta_{w_1}}{2}\left(\omega_{1,t} - \pi_{1,t-1}^{\iota_{w1}}\right)^2 w_{1,t} n_{1,t},$$

$$\Pi_{u_2,t} = \left(1 - \frac{1}{X_{w_2,t}}\right) w_{2,t}\, n_{2,t} - \frac{\eta_{w_2}}{2}\left(\omega_{2,t} - \pi_{2,t-1}^{\iota_{w2}}\right)^2 w_{2,t}\, n_{2,t}.$$

The term Π_t, appearing in the household's budget constraint (eq. 2) is then given by:

$$\Pi_t = \Pi_{u_1,t} + p_{2,t}\Pi_{u_2,t} + \Pi_{r_1,t} + p_{2,t}\Pi_{r_2,t}.$$

B Derivation of the Mixture of Mixture Cubature Kalman Filter

This Appendix describes in detail the derivation of the Mixture of Mixture of Cubature Kalman Filter (MM-CKF). The MM-CKF is based on the Cubature Kalman Filter (CKF) of Arasaratnam and Haykin (2009). The CKF falls into the category of Gauss-Hermite transformation filters, where the moments' propagation and updating are based on numerical integration rules. Differently from the Gauss–Hermite Kalman filter (GHKF) of Ito and Xiong (2000) and the Quadrature Kalman filter (QKF) of Arasaratnam et al. (2007), the number of sigma points scales linearly in the integration dimensions, by the use of symmetric spherical-radial cubature rule. This provides a tool against the curse of dimensionality. The spherical radial cubature rule in Arasaratnam and Haykin (2009) is exact up to order three, meaning that the first moments will be propagated exactly for state-space functions consisting in polynomials up to order three (or well approximated by polynomials up to order three). As pointed out by Särkkä (2013), indeed, the integrations involving second moments will be exact just for state-space functions consisting of polynomials up to order one. It is possible to specify high order Cubature Kalman filters (Jia et al., 2013), but the number of cubature points would scale polynomially in the state dimension. Moreover, some weights may turn negative, possibly giving rise to numerical instability.

Cubature Kalman Filter

The algorithm of the CKF is the following: Assuming $p(x_0^S|\mathbf{y}_{1:0}) = \mathcal{N}(m_{0|0}, P_{0|0})$ the initial distribution of the states, for $t = 1$ to T perform the following steps:

1) **Prediction**

(a) From time $t-1$ posterior density function $p(x_{t-1}^S|\mathbf{y}_{1:t-1}) = \mathcal{N}(m_{t-1|t-1}, P_{t-1|t-1})$ form the augmented filtered cubature points:

$$\begin{pmatrix} \mathcal{X}_{t-1|t-1}^{S^{(i)}} \\ \mathcal{E}_{t-1|t-1}^{(i)} \end{pmatrix} = \begin{pmatrix} m_{t-1|t-1} \\ \mathbb{E}(\boldsymbol{\varepsilon}_t) \end{pmatrix} + \sqrt{\begin{pmatrix} P_{t-1|t-1} & 0 \\ 0 & \mathbb{V}(\boldsymbol{\varepsilon}_t) \end{pmatrix}} \xi^{(i)}$$
$$i = 1, \ldots, 2(n_x^S + n_\varepsilon),$$

where the cubature points $(\xi^{(i)})$ are derived from the spherical-radial rule (Arasaratnam and Haykin, 2009)

$$\xi^{(i)} = \begin{cases} \sqrt{n_x^S + n_\varepsilon}\mathbf{e}_i, & i = 1, \ldots, n_x^S + n_\varepsilon, \\ -\sqrt{n_x^S + n_\varepsilon}\mathbf{e}_{i-n_x^S-n_\varepsilon}, & i = n_x^S + n_\varepsilon + 1, \ldots, 2(n_x^S + n_\varepsilon), \end{cases}$$

and where the $\mathbf{e}_i$'s are the vectors forming the standard basis of $\mathbb{R}^{(n_x^S+n_\varepsilon)}$.

(b) Propagate states cubature points using the second equation in (12):

$$\mathcal{X}_{t|t-1}^{S^{(i)}} = h(\mathcal{X}_{t-1|t-1}^{S^{(i)}}) + R\mathcal{E}_{t-1|t-1}^{(i)}, \quad i = 1, \ldots, 2(n_x^S + n_\varepsilon).$$

(c) Obtain predicted controls cubature points using the first equation in (12):

$$\mathcal{X}_{t|t-1}^{C^{(i)}} = g\left(\mathcal{X}_{t|t-1}^{S^{(i)}}\right), \quad i = 1, \ldots, 2\left(n_x^S + n_\varepsilon\right).$$

(d) Compute predicted means and covariances for states and controls

$$m_{t|t-1}^* \equiv \begin{pmatrix} m_{t|t-1}^S \\ m_{t|t-1}^C \end{pmatrix} = \frac{1}{2(n_x^S + n_\varepsilon)} \sum_{i=1}^{2\left(n_x^S+n_\varepsilon\right)} \begin{pmatrix} \mathcal{X}_{t|t-1}^{S^{(i)}} \\ \mathcal{X}_{t|t-1}^{C^{(i)}} \end{pmatrix},$$

$$P^*_{t|t-1} = \frac{1}{2\left(n_x^S + n_\varepsilon\right)} \sum_{i=1}^{2\left(n_x^S+n_\varepsilon\right)} \left\{ \left[\begin{pmatrix} \mathcal{X}^{S^{(i)}}_{t|t-1} \\ \mathcal{X}^{C^{(i)}}_{t|t-1} \end{pmatrix} - \begin{pmatrix} m^S_{t|t-1} \\ m^C_{t|t-1} \end{pmatrix} \right] \left[\begin{pmatrix} \mathcal{X}^{S^{(i)}}_{t|t-1} \\ \mathcal{X}^{C^{(i)}}_{t|t-1} \end{pmatrix} - \begin{pmatrix} m^S_{t|t-1} \\ m^C_{t|t-1} \end{pmatrix} \right] \right\}'.$$

2) **Updating**

(a) Form the predicted states and controls cubature points:

$$\mathcal{X}^{*(i)}_{t|t-1} = m^*_{t|t-1} + \sqrt{P^*_{t|t-1}}\zeta^{(i)}, \quad i = 1, \ldots, 2(n_x^S + n_x^C).$$

(b) Obtain predicted observations cubature points through the measurement equation (13):

$$\mathcal{Y}^{(i)}_{t|t-1} = A + B\mathcal{X}^{*(i)}_{t|t-1}, \quad i = 1, \ldots, 2\left(n_x^S + n_x^C\right).$$

(c) Compute predicted observables mean, covariance and cross-covariance between the states and observables:

$$\bar{\mathcal{Y}}_{t|t-1} = \frac{1}{2\left(n_x^S + n_x^C\right)} \sum_{i=1}^{2\left(n_x^S+n_x^C\right)} \mathcal{Y}^{(i)}_{t|t-1},$$

$$\mathcal{F}_{t|t-1} = \frac{1}{2\left(n_x^S + n_x^C\right)} \sum_{i=1}^{2\left(n_x^S+n_x^C\right)} \left(\mathcal{Y}^{(i)}_{t|t-1} - \bar{\mathcal{Y}}_{t|t-1}\right)\left(\mathcal{Y}^{(i)}_{t|t-1} - \bar{\mathcal{Y}}_{t|t-1}\right)' + \mathbb{V}(u_t),$$

$$\mathcal{P}^{xy}_{t|t-1} = \frac{1}{2(n_x^S + n_x^C)} \sum_{i=1}^{2\left(n_x^S+n_x^C\right)} \left(\mathcal{X}^{*(i)}_{t|t-1} - m^*_{t|t-1}\right)\left(\mathcal{Y}^{(i)}_{t|t-1} - \bar{\mathcal{Y}}_{t|t-1}\right)'.$$

(d) Compute Kalman gain to obtain the new filtered mean and covariance for states and controls:

$$\mathcal{K}_t = \mathcal{P}^{xy}_{t|t-1}\left(\mathcal{F}_{t|t-1}\right)^{-1},$$

$$m^*_{t|t} = m^*_{t|t-1} + \mathcal{K}_t(y_t - \bar{\mathcal{Y}}_{t|t-1}),$$

$$P^*_{t|t} = P^*_{t|t-1} - \mathcal{P}^{xy}_{t|t-1}\left(\mathcal{F}_{t|t-1}\right)^{-1}\left(\mathcal{P}^{xy}_{t|t-1}\right)'.$$

From $m^*_{t|t}$ and $P^*_{t|t}$ the n_x^S states entries are retained to have $m_{t|t}$ and $P_{t|t}$ to be

used in the following iteration.

Mixture of Mixture of Cubature Kalman Filter

The MM-CKF described in Section V is based on the CKF. This mixture of structural errors allows us to disentangle the structural shock that experiences the large negative (positive) impulse. We now explain in detail the MM-CKF.

Assume $p\left(x_0^S|\mathbf{y}_{1:0}\right) = \mathcal{N}\left(m_{0|0}, P_{0|0}\right)$ as the initial distribution of the states, and $G_0 = 1$. For $t = 1, \ldots, T$ and for each filtered component $g = 1, \ldots, G_{t-1}$ in

$$p\left(\mathbf{x}_{t-1}|\mathbf{y}_{1:t-1}\right) = \sum_{g=1}^{G_{t-1}} p\left(\mathbf{x}_{t-1}|\kappa_{t-1}^g, \mathbf{y}_{1:t-1}\right) p\left(\kappa_{t-1}^g|\mathbf{y}_{1:t-1}\right) = \sum_{g=1}^{G_{t-1}} \mathcal{N}\left(m_{t-1|t-1}^g, P_{t-1|t-1}^g\right) w_{t-1|t-1}^g.$$

perform the following steps:

1) **Prediction**

   (a) Split each filter g in K densities with predicted weights $\tilde{w}_{t|t-1}^{g,k} = w_{t-1|t-1}^g \psi_{k,t}$, $k = 1, \ldots, K$, assuming noise from component $\boldsymbol{\varepsilon}_t^k$.

   (b) For each shock component $k = 1, \ldots, K$ form the augmented filtered cubature points:

$$\begin{pmatrix} \mathcal{X}_{t-1|t-1}^{g,k,S^{(i)}} \\ \mathcal{E}_{t-1|t-1}^{g,k,(i)} \end{pmatrix} = \begin{pmatrix} m_{t-1|t-1}^g \\ \mathbb{E}(\boldsymbol{\varepsilon}_t^k) \end{pmatrix} + \sqrt{\begin{pmatrix} P_{t-1|t-1}^g & 0 \\ 0 & \mathbb{V}(\boldsymbol{\varepsilon}_t^k) \end{pmatrix}} \xi^{(i)}$$
$$i = 1, \ldots, 2(n_x^S + n_{\boldsymbol{\varepsilon}}).$$

   (c) Propagate states cubature points using Equation (12):

$$\mathcal{X}_{t|t-1}^{g,k,S^{(i)}} = h\left(\mathcal{X}_{t-1|t-1}^{g,k,S^{(i)}}\right) + R\mathcal{E}_{t-1|t-1}^{g,k,(i)}, \quad i = 1, \ldots, 2(n_x^S + n_\varepsilon).$$

   (d) Obtain predicted controls cubature points using Equation (12):

$$\mathcal{X}_{t|t-1}^{g,k,C^{(i)}} = g\left(\mathcal{X}_{t|t-1}^{g,k,S^{(i)}}\right), \quad i = 1, \ldots, 2(n_x^S + n_\varepsilon).$$

(e) Compute predicted means and covariances for states and controls:

$$m^{*,g,k}_{t|t-1} \equiv \begin{pmatrix} m^{g,k,S}_{t|t-1} \\ m^{g,k,C}_{t|t-1} \end{pmatrix} = \frac{1}{2\left(n^S_x + n_\varepsilon\right)} \sum_{i=1}^{2(n^S_x+n_\varepsilon)} \begin{pmatrix} \mathcal{X}^{g,k,S^{(i)}}_{t|t-1} \\ \mathcal{X}^{g,k,C^{(i)}}_{t|t-1} \end{pmatrix},$$

$$P^{*,g,k}_{t|t-1} = \frac{1}{2\left(n^S_x + n_\varepsilon\right)} \sum_{i=1}^{2\left(n^S_x+n_\varepsilon\right)} \left\{ \left[\begin{pmatrix} \mathcal{X}^{g,k,S^{(i)}}_{t|t-1} \\ \mathcal{X}^{g,k,C^{(i)}}_{t|t-1} \end{pmatrix} - \begin{pmatrix} m^{g,k,S}_{t|t-1} \\ m^{g,k,C}_{t|t-1} \end{pmatrix} \right] \left[\begin{pmatrix} \mathcal{X}^{S^{(i)}}_{t|t-1} \\ \mathcal{X}^{C^{(i)}}_{t|t-1} \end{pmatrix} - \begin{pmatrix} m^{g,k,S}_{t|t-1} \\ m^{g,k,C}_{t|t-1} \end{pmatrix} \right] \right\}'.$$

2) **Updating**

(a) For each component $\{g, k\}$ form the predicted states and controls cubature points:

$$\mathcal{X}^{*,g,k,(i)}_{t|t-1} = m^{*,g,k}_{t|t-1} + \sqrt{P^{*,g,k}_{t|t-1}}\zeta^{(i)}, \quad i = 1, \ldots, 2(n^S_x + n^C_x).$$

(b) Obtain predicted observables cubature points through the measurement equation (13):

$$\mathcal{Y}^{g,k,(i)}_{t|t-1} = A + B\mathcal{X}^{*,g,k,(i)}_{t|t-1}, \quad i = 1, \ldots, 2(n^S_x + n^C_x).$$

(c) Compute predicted observables mean, covariance and cross-covariance between states and observables:

$$\bar{\mathcal{Y}}^{g,k}_{t|t-1} = \frac{1}{2(n^S_x + n^C_x)} \sum_{i=1}^{2(n^S_x+n^C_x)} \mathcal{Y}^{g,k,(i)}_{t|t-1},$$

$$\mathcal{F}^{g,k}_{t|t-1} = \frac{1}{2\left(n^S_x + n^C_x\right)} \sum_{i=1}^{2\left(n^S_x+n^C_x\right)} \left(\mathcal{Y}^{g,k,(i)}_{t|t-1} - \bar{\mathcal{Y}}^{g,k}_{t|t-1}\right)\left(\mathcal{Y}^{g,k,(i)}_{t|t-1} - \bar{\mathcal{Y}}^{g,k}_{t|t-1}\right)' + \mathbb{V}(u_t),$$

$$\mathcal{P}^{g,k,xy}_{t|t-1} = \frac{1}{2\left(n^S_x + n^C_x\right)} \sum_{i=1}^{2(n^S_x+n^C_x)} \left(\mathcal{X}^{*,g,k,(i)}_{t|t-1} - m^{*,g,k}_{t|t-1}\right)\left(\mathcal{Y}^{(i)}_{t|t-1} - \bar{\mathcal{Y}}^{g,k}_{t|t-1}\right)'.$$

(d) Compute Kalman gain to obtain new filtered mean and covariance for states and controls:

$$\mathcal{K}^{g,k}_t = \mathcal{P}^{g,k,xy}_{t|t-1}\left(\mathcal{F}^{g,k}_{t|t-1}\right)^{-1},$$

$$m_{t|t}^{*,g,k} = m_{t|t-1}^{*,g,k} + \mathcal{K}_t^{g,k}\left(y_t - \bar{\mathcal{Y}}_{t|t-1}^{g,k}\right),$$

$$P_{t|t}^{*,g,k} = P_{t|t-1}^{*,g,k} - \mathcal{P}_{t|t-1}^{g,k,xy}\left(\mathcal{F}_{t|t-1}^{g,k}\right)^{-1}\left(\mathcal{P}_{t|t-1}^{g,k,xy}\right)'.$$

From $m_{t|t}^{*,g,k}$ and $P_{t|t}^{g,k,*}$ the n_x^S states entries are retained to have $m_{t|t}^{g,k}$ and $P_{t|t}^{g,k}$.

3) **Weights updating**

(a) Weights are updated using Bayes' rule:

$$\tilde{w}_{t|t}^{g,k} = \frac{\tilde{w}_{t|t-1}^{g,k}\mathcal{N}\left(\mathbf{y}_t; \bar{\mathcal{Y}}_{t|t-1}^{g,k}, \mathcal{F}_{t|t-1}^{g,k}\right)}{\sum_{g=1}^{G_{t-1}}\sum_{k=1}^{K}\tilde{w}_{t|t-1}^{g,k}\mathcal{N}\left(\mathbf{y}_t; \bar{\mathcal{Y}}_{t|t-1}^{g,k}, \mathcal{F}_{t|t-1}^{g,k}\right)}.$$

4) **Collapsing (only if $G_{t-1}K > \bar{G}$)**

(a) Components weights $\tilde{w}_{t|t}^{g,k}$ are sorted in descending order.

(b) The first $\bar{G}$ components and their respective means and covariances $m_{t|t}^{g,k}$ and $P_{t|t}^{g,k}$ are retained and their indices $\{g,k\}$ are relabeled with $1,\ldots,\bar{G}$.

(c) If the smallest retained weight $\tilde{w}_{t|t}^{\bar{G}} < \tilde{w}_{threshold}$ resampling is conducted from the $\bar{G}$ retained mixands using probabilities proportional to $\tilde{w}_{t|t}^{g}$, $g = 1,\ldots,\bar{G}$. Weights are then set to $\frac{1}{\bar{G}}$ and identical mixands are collapsed.

(d) Next period filtering weights are finally obtained by normalization:

$$w_{t|t}^{g} = \frac{\tilde{w}_{t|t}^{g}}{\sum_{g=1}^{G_t}\tilde{w}_{t|t}^{g}}.$$

The likelihood function is then approximated by:

$$p\left(\mathbf{y}_{1:T}|\theta\right) = \prod_{t=1}^{T} p\left(\mathbf{y}_t|\mathbf{y}_{1:t-1};\theta\right) \approx \prod_{t=1}^{T}\mathcal{N}\left(\mathbf{y}_t; \bar{\mathcal{Y}}_{t|t-1}, \mathcal{F}_{t|t-1}\right),$$

where $\bar{\mathcal{Y}}_{t|t-1} = \sum_{g=1}^{G_{t-1}}\sum_{k=1}^{K}\tilde{w}_{t|t-1}^{g,k}\bar{\mathcal{Y}}_{t|t-1}^{g,k}$ and:

$$\mathcal{F}_{t|t-1} = \sum_{g=1}^{G_{t-1}}\sum_{k=1}^{K}\tilde{w}_{t|t-1}^{g,k}\left[\mathcal{F}_{t|t-1}^{g,k} + \left(\bar{\mathcal{Y}}_{t|t-1}^{g,k} - \bar{\mathcal{Y}}_{t|t-1}\right)\left(\bar{\mathcal{Y}}_{t|t-1}^{g,k} - \bar{\mathcal{Y}}_{t|t-1}\right)'\right].$$

C Data Construction

Value added

To obtain the series of value added in the two sectors, we take the total real value added (i.e., Gross Domestic Product), and the shares of the two sectors. Gross Domestic Product (GDP) is retrieved from the U.S. Bureau of Economic Analysis series GDPC1. The series is seasonally adjusted and is expressed as billions of chained 2012 dollars. The GDP is divided by the Civilian Noninstitutional Population (series CNP16OV from the U.S. Bureau of Labor Statistics) to transform it in per capita terms.
Sectoral shares data is obtained from the GDP-by-industry accounts from the U.S. Bureau of Economic Analysis. The share of the general sector is obtained by summing the shares of:

- Agriculture, forestry, fishing, and hunting; Mining; Utilities; Construction; Manufacturing; Wholesale trade; Retail trade; Transportation and warehousing; Information; Finance, insurance, real estate, rental, and leasing; Professional and business services; Educational services, health care, and social assistance; Other services, except government; Federal government; State and local government.

The share of the Leisure and Hospitality sector is equal to the share of the following sectors:

- Arts, entertainment, recreation, accommodation, and food services.

The value added in the two sectors is finally obtained by multiplying the total value added by these shares. Data is available annually until 2005:Q1 and at quarterly frequencies afterward. The missing quarters are handled as missing data by the MM-CKF, setting to zero the corresponding Kalman gain entries. The data spans from 1985:Q1 to 2021:Q4.

Inflation

Sectoral data on prices are collected by the U.S. Bureau of Economic Analysis in the GDP-by-industry accounts. For each sector, chain-type price indexes are collected, with 2012 being the reference year. As for value-added by sectors, quarterly data is only available starting from 2005:Q1. Only one out of four quarterly inflation rates are therefore assumed

to be observed for each year before 2005 and it is assumed to be equal to the yearly rate divided by four. The other observations are treated as missing. The data spans from 1985:Q1 to 2021:Q4.

Consumption

Aggregate real consumption in billions of chained 2012 dollars is provided by the U.S. Bureau of Economic Analysis in the PCECC96 series. The series is seasonally adjusted and it spans from 1985:Q1 to 2021:Q4. The series is divided by the Population Level (CNP16OV) to get per capita consumption.

Investment

Real Gross Private Domestic Investment is retrieved from the U.S. Bureau of Economic Analysis series GPDIC1. It is seasonally adjusted and measured in billions of chained 2012 dollars and it spans from 1985:Q1 to 2021:Q4. The series is divided by the Population Level (CNP16OV) to get per capita investment.

Hours worked

Data on hours worked across industries is obtained from the U.S. Bureau of Labor Statistics's Current Employment Statistics (Establishment Survey). In Table B-7, the average weekly hours and overtime of production and nonsupervisory employees on private nonfarm payrolls is collected, while the number of employees on nonfarm payrolls for each industry is found in Table B-1. The original monthly series are filtered to the quarterly frequency by applying the arithmetic mean. All series are seasonally adjusted. The per capita weekly hours worked in each sector are obtained by multiplying the average hours by employment and dividing them by the Population Level (CNP16OV). The data spans from 1985:Q1 to 2021:Q4.

Wages

Data on sectoral nominal wages is retrieved from the Current Employment Statistics (Establishment Survey) provided by U.S. Bureau of Labor Statistics. Average hourly earnings of production and nonsupervisory employees for the various industries are found

in Table B-8. Monthly seasonally adjusted data is averaged to obtain quarterly figures. Nominal wages for aggregate subsets of sectors is obtained as a weighted average of wages with respect to hours worked in that sectors. We differentiate logged data to get nominal wage inflation. The data spans from 1985:Q1 to 2021:Q4.

Interest rate

The nominal short-term interest rate is measured as the 3-Month Treasury Bill yield in the secondary market. The daily measurements are averaged and divided by four to get the quarterly interest rate. The data spans from 1985:Q1 to 2021:Q4.

D Steady State

Here we derive the steady state of the model. Variables without the time subscript denote steady-state values. The model is solved around a steady state with zero inflation. Utilization rates are normalized to one at the steady state and all adjustment costs are zero. Moreover, markups are equal to their flexible-price value, namely:

$$\pi_1 = 1, \quad \pi_2 = 1, \quad u_{k_1} = 1, \quad u_{k_2} = 1,$$

$$\Psi_{k_1} = 0, \quad \Psi_{k_2} = 0, \quad \Psi_{u_1} = 0, \quad \Psi_{u_2} = 0,$$

$$X_1 = \frac{\epsilon_{\pi_1}}{\epsilon_{\pi_1} - 1}, \quad X_2 = \frac{\epsilon_{\pi_2}}{\epsilon_{\pi_2} - 1}, \quad X_{w_1} = \frac{\epsilon_{w_1}}{\epsilon_{w_1} - 1}, \quad X_{w_2} = \frac{\epsilon_{w_2}}{\epsilon_{w_2} - 1}.$$

The parameter R_{ss}, appearing in the Taylor rule and pinning down the steady state for the unconstrained interest rate R_{unc}, is calibrated to be the root of the barrier polynomial $R = c_0 + c_1 R_{unc} + c_2 R_{unc}^2$ (the economically admissible one of the two), so that:

$$R_{unc} = R_{ss},$$

and

$$R = \frac{1}{\beta}.$$

The auxiliary variables ζ_0, ζ_1, ζ_2 and ζ_3 are defined for the sake of convenience. The variables ζ_0 and ζ_1 are respectively equal to $\frac{k_1}{Y_1}$ and $\frac{k_2}{Y_2}$, while ζ_2 and ζ_3 stand for $\frac{c_1}{Y_1}$ and

$\frac{c_2}{Y_2}$, respectively. It holds that:

$$\zeta_0 = \frac{\alpha_1\beta}{X_1(1-\beta(1-\delta_{k_1}))}, \quad \zeta_1 = \frac{\alpha_2\beta}{X_2(1-\beta(1-\delta_{k_2}))}, \quad \zeta_3 = 1,$$

$$n_2 = \left(\frac{1-\alpha_2}{X_2 X_{w_2}}\frac{1}{\zeta_3}\frac{j^{ss}}{\phi_2^{ss}}\right)^{\frac{1}{1+\nu_2}}, \quad Y_2 = n_2\zeta_1^{\frac{\alpha_2}{1-\alpha_2}}, \quad k_2 = \zeta_1 Y_2, \quad c_2 = \zeta_3 Y_2.$$

The ratio between c_1 and p_2 can be easily found as:

$$c_1/p_2 = \frac{c_2}{j^{ss}}.$$

Then, by the market clearing for Sector $\mathcal{S}_1$,

$$Y_1/p_2 = \frac{c_1/p_2 + \delta_{k_2}k_2}{1-\delta_{k_1}\zeta_0},$$

so that

$$\zeta_2 = \frac{c_1/p_2}{Y_1/p_2}, \quad n_1 = \left(\frac{1-\alpha_1}{X_1 X_{w_1}}\frac{1}{\zeta_2}\frac{1}{\phi_1^{ss}}\right)^{\frac{1}{1+\nu_1}}, \quad Y_1 = n_1\zeta_0^{\frac{\alpha_1}{1-\alpha_1}}, \quad k_1 = \zeta_0 Y_1,$$

$$c_1 = \zeta_2 Y_1, \quad u_{c_1} = \frac{1}{c_1}, \quad u_{c_2} = \frac{j^{ss}}{c_2}, \quad w_1 = \phi_1^{ss} n_1^{\nu_1}\frac{X_{w_1}}{u_{c_1}},$$

$$w_2 = \phi_2^{ss} n_2^{\nu_2}\frac{X_{w_2}}{u_{c_2}}, \quad p_2 = \frac{u_{c_2}}{u_{c_1}}, \quad \Pi_{r_1} = \left(1-\frac{1}{X_1}\right)Y_1, \quad \Pi_{r_2} = \left(1-\frac{1}{X_2}\right)Y_2,$$

$$\Pi_{u_1} = \left(1-\frac{1}{X_{w_1}}\right)w_1 n_1, \quad \Pi_{u_2} = \left(1-\frac{1}{X_{w_2}}\right)w_2 n_2, \quad \pi = \pi_1^{\left(\frac{Y_1}{Y_1+p_2Y_2}\right)}\pi_2^{\left(\frac{p_2Y_2}{Y_1+p_2Y_2}\right)} = 1,$$

$$a_{z_1} = 1, \quad a_{z_2} = 1, \quad a_j = j^{ss}, \quad a_s = 1, \quad \phi_1 = \phi_1^{ss}, \quad \phi_2 = \phi_2^{ss}.$$

E Alternative strategies

Stability of parameters

In this Appendix we show that ignoring the modellization of large shocks during the pandemic quarters biases the estimation of the model parameters; differently, we show that including large shocks makes inference on parameters feasible. To do so, we re-estimate the model on a pre-pandemic dataset that starts from 1985:Q1 and ends in 2019:Q4, before the outbreak of the pandemic in the US. This exercise is conducted using the same prior specification of the baseline estimation presented in the paper.

As shown in Table 4, our modellization of large shocks (Baseline) gives parameter estimates that remain stable with respect to the pre-pandemic estimation (No-Pandemic). The values at the posterior mean in these two cases report small movements, with minor differences given by the information carried by the pandemic quarters. Furthermore, we run an estimation (No Large Shocks) that ignores the presence of large shocks, meaning that all the shocks are always assumed to come from the ordinary component. In this case the parameters at the posterior mean are greatly affected by the last pandemic observations, and they move substantially from the pre-pandemic values. As visible from the *No Large Shocks* column in Table 4 ignoring large shocks biases upward the standard deviations of the shocks, drives down the parameters related to habits in consumption (h_1 and h_2), shrinks the utilization cost parameters ($\eta_{u,1}$ and $\eta_{u,2}$) towards zero and revises upward the estimates for the capital adjustment costs ($\eta_{k,1}$ and $\eta_{k,2}$). Also the exogenous persistence parameters change dramatically.

Table 4: Estimation Results with alternative specifications. Note: The table reports the parameter's name (Full Name) with the associated symbol (Symbol). The table then reports the posterior mean for the estimated parameters in case of the baseline estimation (Baseline), the estimation that ends at 2019:Q4 (No-Pandemic), the estimation that goes up to 2021:Q4 but does not model large shocks (No Large Shocks).

Full Name	Symbol	Baseline	No-Pandemic	No Large Shocks
Habits $\mathcal{S}_1$	h_1	0.79	0.79	0.42
Habits $\mathcal{S}_2$	h_2	0.91	0.87	0.90
Price rigidity $\mathcal{S}_1$	θ_1	0.70	0.71	0.71
Price rigidity $\mathcal{S}_2$	θ_2	0.57	0.51	0.52
Inverse Frisch el. $\mathcal{S}_1$	ν_1	0.25	0.36	0.30

Table 4 – *Continued from previous page*

Full Name	Symbol	Baseline	No-Pandemic	No Large Shocks
Inverse Frisch el. $\mathcal{S}_2$	ν_2	0.34	0.40	0.26
Taylor rule inertia	r_R	0.70	0.66	0.66
Taylor rule output	r_Y	0.14	0.14	0.06
Taylor rule inflation	r_π	1.99	1.94	2.08
Price indexation $\mathcal{S}_1$	ι_{π_1}	0.82	0.80	0.67
Price indexation $\mathcal{S}_2$	ι_{π_2}	0.82	0.80	0.74
Persistence Prod. $\mathcal{S}_1$	ρ_{z_1}	0.99	0.99	0.93
Persistence Prod. $\mathcal{S}_2$	ρ_{z_2}	0.18	0.29	0.38
Persistence Intratemp.	ρ_j	0.35	0.32	0.22
Persistence Lab. Supply $\mathcal{S}_1$	ρ_{ϕ_1}	0.73	0.76	0.34
Persistence Lab. Supply $\mathcal{S}_2$	ρ_{ϕ_2}	0.15	0.10	0.70
Persistence Intertemp.	ρ_ζ	0.67	0.66	0.82
Wage rigidity $\mathcal{S}_1$	θ_{w_1}	0.84	0.85	0.76
Wage rigidity $\mathcal{S}_2$	θ_{w_2}	0.68	0.68	0.72
Wage indexation $\mathcal{S}_1$	ι_{w_1}	0.88	0.81	0.90
Wage indexation $\mathcal{S}_2$	ι_{w_2}	0.77	0.70	0.08
Uiliz. adj.cost $\mathcal{S}_1$	$\eta_{u,1}$	0.92	0.89	0.60
Uiliz. adj.cost $\mathcal{S}_2$	$\eta_{u,2}$	0.22	0.22	0.37
Cap. adj.cost $\mathcal{S}_1$	η_{k_1}	13.38	11.53	13.09
Cap. adj.cost $\mathcal{S}_2$	η_{k_2}	12.10	5.38	10.36
St.Dev. Prod. $\mathcal{S}_1$	$100 \times \sigma_{z_1}$	0.74	0.71	0.81
St.Dev. Temp. Mon. Policy	$100 \times \sigma_e$	0.29	0.24	0.33
St.Dev. Prod. $\mathcal{S}_2$	$100 \times \sigma_{z_2}$	1.39	1.19	3.48
St.Dev. Intratemp.	$100 \times \sigma_j$	10.98	7.30	60.67
St.Dev. Pers. Mon. Policy	$100 \times \sigma_s$	5.42	4.86	7.72
St.Dev. Lab. Supply $\mathcal{S}_1$	$100 \times \sigma_{\phi_1}$	6.14	6.38	8.33
St.Dev. Lab. Supply $\mathcal{S}_2$	$100 \times \sigma_{\phi_2}$	73.51	64.18	29.95
St.Dev. Pref.	$100 \times \sigma_\zeta$	2.97	2.88	1.91

Student's t shocks

We show that a Student's t specification can hardly generate the economic shocks found in the paper. To this end, we evaluate the likelihood of the shocks under the hypothesis that they are drawn from uncorrelated Student's t distributions with 2, 5, and 20 degrees of freedom ($\nu = 2, 5, 20$). Figure 10 it is shown the log-density of a multivariate Student's t with a diagonal covariance matrix, evaluated at the standardized shocks filtered by the MM-CKF, at each time point, namely:

$$f_{\nu}^{t}(\tilde{\varepsilon}_t) = \frac{\Gamma\left[(\nu + n_{\varepsilon})/2\right]}{\Gamma(\nu/2)\nu^{n_{\varepsilon}/2}\pi^{n_{\varepsilon}/2}} \left[1 + \frac{1}{\nu}\tilde{\varepsilon}_t^{'}\tilde{\varepsilon}_t\right]^{-(\nu+n_{\varepsilon})/2},$$

where $\Gamma(\cdot)$ is the Gamma function. Consistently with the main text, n_{ε} is the number of structural shocks of the model and $\tilde{\varepsilon}_t$ are the standardized shocks occurring at time t, namely $\left(\tilde{\varepsilon}_t = \frac{\varepsilon_t}{\boldsymbol{\sigma}}\right)$. As Figure 10 shows, in the last two quarters (2020:Q2 and 2020:Q3) the value of f_{ν}^{t} drops substantially, indicating that the shocks ($\tilde{\varepsilon}_t$) lie in the tail density. For the most leptokurtic case, $\nu = 2$, it is shown that the log-density value, in the last two quarters, is around -30, while in usual times it hovers around a value of -9. For the case of higher degrees of freedom ($\nu = 5$ and $\nu = 20$), these observations are further in the tails, and the log-density values in these quarters are even lower. We have to underline that, if a Student's t with low degrees of freedom can draw one large shock as the one of 2020 with non-negligible probability, the likelihood of a Student's t distribution drawing many large shocks at the same time is low, and this is the reason why the value density value drops so much.

F The Approximate Conditional Optimal Particle Filter

The Conditionally Optimal Particle Filter (COPF), see Herbst and Schorfheide (2015) and Aruoba et al. (2021), requires an exact expression for conditionally-optimal proposal density. This can be easily derived just in few special cases including: linear state transitions and piecewise-linear state transitions. Specifically, Aruoba et al. (2021) show that when the DSGE solution produces piecewise-linear state transition equations, the conditionally optimal density takes the form of truncated normal mixtures.

In our model solution, the state transition is a second order polynomial in the states and,

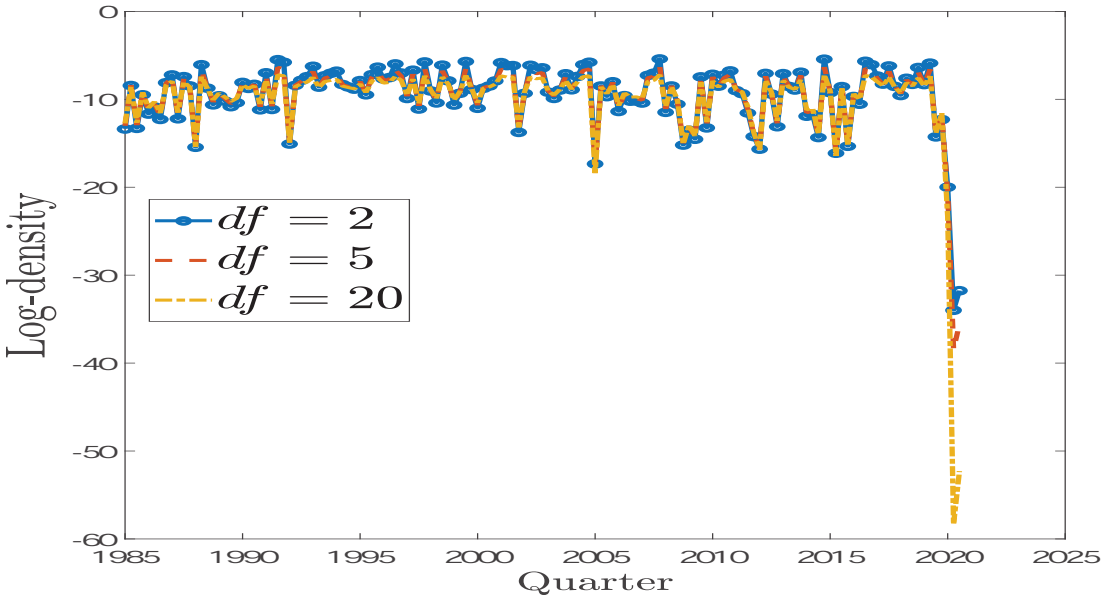

Figure 10: Log-density of shocks under a Student's t distribution.

unfortunately, an exact expression for the conditionally optimal density is not available and the COPF cannot be applied. As an approximation, we propose the Approximate Conditionally Optimal Particle Filter (ACOPF) which the conditionally-approximate density is derived with a CKF step. More specifically:

$$p(\mathbf{x}_t|\mathbf{x}_{t-1}^j, \mathbf{y}_t) \approx \tilde{p}(\mathbf{x}_t|\mathbf{x}_{t-1}^j, \mathbf{y}_t) = \mathcal{N}\left(\mathbf{x}_{t|t}^{j,CKF}, P_{t|t}^{j,CKF}\right),$$

where $\mathbf{x}_{t|t}^{j,CKF}$ and $P_{t|t}^{j,CKF}$ represent respectively the filtered means and covariances, of the unobserved states, obtained from a run of the CKF on the latest observation $\mathbf{y}_t$, this filter is also known as Cubature Particle Filter (CPF).

In the context of DSGE models, the optimal importance density approximation using Gaussian filters have been proposed, among others, by Amisano and Tristani (2010) (Extended Kalman Filter) and by Andreasen (2011) (Central Difference Kalman filter). By using an importance density proposal $g_t(\mathbf{x}_t|\mathbf{x}_{t-1}^j, \mathbf{y}_t) \neq p(\mathbf{x}_t|\mathbf{x}_{t-1}^j)$, the importance weight

$$w_t^j = \frac{p(\mathbf{y}_t|\mathbf{x}_t^j)p(\mathbf{x}_t^j|\mathbf{x}_{t-1}^j)}{g_t(\mathbf{x}_t^j|\mathbf{x}_{t-1}^j, \mathbf{y}_t)},$$

must be evaluated. In our case, as in Andreasen (2011), the density $p(\mathbf{x}_t^j|\mathbf{x}_{t-1}^j)$ is degenerate, given that the shocks enter contemporaneously for just some state variables, i.e. the loading matrix R displays null lines and $R\mathbb{V}(\varepsilon_t)R'$ is singular. To circumvent this problem, exactly as in Andreasen (2011), the proposal is split is two parts. The first one propagates the states corresponding to the singular lines deterministically through the transition functions. The second part updates the states corresponding to the non singular lines by a run of the CKF. The importance weight for each particle is then calculated only evaluating the non-degenerate part of the density corresponding to the non-degenerate states.

G Miscellanea

Detailed Monte Carlo results

Table 5 reports the full version of Table 1 in the main text.

Table 5: Full table. RMSE of the Monte Carlo experiment for $N = 100$ replications of the Two-Sector model with large shocks. Note: The Table reports the full name (Full Name) with the associated symbol (Symbol). The filters are: Kalman filter (KF); Bootstrap Particle Filter with 40000 particles (BPF); Auxiliary Particle Filter with 40000 particles (APF); the Approximate Optimal Particle Filter with 400 and 4000 particles (ACOPF(400), ACOPF(40000)); and the Mixture of Mixture of Cubature Kalman Filter (MM-CKF) with four components ($\bar{G} = 4$).

Full Name	Symbol	KF	BPF	APF	ACOPF(400)	ACOPF(4000)	MM-CKF
Wage $\mathcal{S}_1$	w_1	3.00	0.88	1.00	1.00	1.10	0.98
Int. rate	r_{unc}	0.49	0.07	0.06	0.05	0.05	0.08
Lab. Supply $\mathcal{S}_1$	a_{t_1}	1.30	1.20	1.20	1.50	1.20	0.60
Wage $\mathcal{S}_2$	w_2	0.23	0.27	0.27	0.20	0.18	0.20
Lab. supply $\mathcal{S}_2$	a_{t_2}	14.00	9.90	9.80	9.70	9.50	8.80
Prod. $\mathcal{S}_1$	a_{z_1}	2.70	0.89	1.00	1.00	1.10	0.94
Prod. $\mathcal{S}_2$	a_{z_2}	0.09	0.16	0.16	0.15	0.13	0.08
Persistent MP	a_s	6.00	2.20	2.30	2.80	2.40	0.99
Consumption $\mathcal{S}_1$	c_1	3.00	0.94	1.10	1.10	1.10	1.00
Intertemp. shock	a_ζ	0.98	0.51	0.51	0.58	0.52	0.23
Intratemp. shock	a_j	1.20	1.70	1.60	1.70	1.60	1.10
Inflation $\mathcal{S}_1$	π_1	0.05	0.04	0.04	0.02	0.02	0.02
Consumption $\mathcal{S}_2$	c_2	2.60	1.90	1.80	2.10	1.90	1.00

Table 5 – *Continued from previous page*

Full Name	Symbol	KF	BPF	APF	ACOPF(400)	ACOPF(4000)	MM-CKF
Inflation $\mathcal{S}_2$	π_2	0.06	0.18	0.17	0.05	0.04	0.02
Capital $\mathcal{S}_1$	k_1	4.30	1.10	1.30	1.40	1.20	1.10
Capital $\mathcal{S}_2$	k_2	2.30	2.50	2.50	2.60	2.50	2.60
MP shock	ϵ_e	0.08	0.03	0.03	0.03	0.03	0.03
Relative price	p_2	5.20	1.30	1.50	1.60	1.40	1.20
Investment	$invest$	4.00	1.30	1.40	1.50	1.30	1.10
Production $\mathcal{S}_1$	Y_1	3.40	0.93	1.10	1.10	1.10	1.00
Production $\mathcal{S}_2$	Y_2	2.50	1.90	1.70	2.10	1.90	0.99
Hours $\mathcal{S}_1$	n_1	0.39	0.44	0.45	0.48	0.39	0.20
Hours $\mathcal{S}_2$	n_2	2.60	1.90	1.70	2.00	1.90	0.84
Total output	GDP	3.40	0.93	1.10	1.10	1.10	1.00
Markup $\mathcal{S}_1$	X_1	0.16	0.10	0.09	0.09	0.08	0.05
Marg. ut. $\mathcal{S}_2$	u_{c_2}	2.50	1.00	1.00	0.72	0.67	0.98
Markup $\mathcal{S}_2$	X_2	0.09	0.15	0.15	0.07	0.07	0.06
Inflation	π	0.04	0.04	0.04	0.02	0.01	0.001
Profits retailers	Π_r	3.80	1.40	1.40	1.40	1.30	1.10
Cap. adj. Cost	Ψ_k	0.25	0.11	0.10	0.08	0.08	0.08
Wage markup $\mathcal{S}_1$	X_{w_1}	1.10	0.85	0.85	0.99	0.86	0.43
Wage markup $\mathcal{S}_2$	X_{w_2}	15.00	9.50	9.50	9.00	8.90	8.60
Profits unions	Π_u	17.00	19.00	19.00	13.00	12.00	7.20
Int. rate	R	0.14	0.04	0.04	0.02	0.02	0.02
Marg. ut. $\mathcal{S}_1$	u_{c_1}	3.80	0.99	1.10	1.30	1.10	1.00
Rental rate $\mathcal{S}_1$	r_{k_1}	1.00	0.50	0.48	0.62	0.50	0.30
Utilization $\mathcal{S}_1$	u_{k_1}	0.08	0.05	0.05	0.06	0.05	0.03
Rental rate $\mathcal{S}_2$	r_{k_2}	0.39	0.33	0.34	0.33	0.30	0.42
Utilization $\mathcal{S}_2$	u_{k_2}	1.40	1.00	1.10	1.00	0.93	1.40
Wage infl. $\mathcal{S}_1$	ω_1	0.03	0.05	0.05	0.02	0.02	0.01
Wage infl. $\mathcal{S}_2$	ω_2	0.13	0.24	0.24	0.07	0.08	0.01
Uiliz. adj.cost $\mathcal{S}_1$	Ψ_{u_1}	0.00	0.00	0.00	0.00	0.00	0.00
Uiliz. adj.cost $\mathcal{S}_2$	Ψ_{u_2}	0.05	0.04	0.04	0.04	0.04	0.05

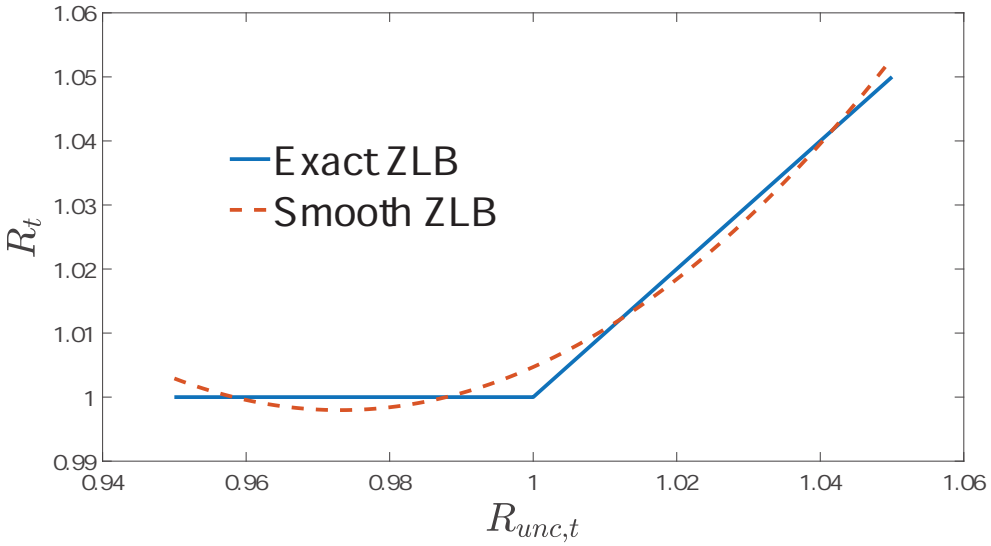

Figure 11: The exact and the smooth zero lower bound.

Table 6: Coefficients of the smooth barrier polynomial.

c_0	c_1	c_2
9.79	-18.07	9.28

Constraining polynomial

As detailed in the main text, we approximate the lower bound on the nominal interest rate by using a smooth barrier polynomial. The form of the approximating polynomial is the following:

$$R_t = c_0 + c_1 R_{unc,t} + c_2 R_{unc,t}^2.$$

The values for the c_0, c_1 and c_2 coefficients are chosen by performing a least squares regression of the ideal zero lower bound ($R_t = max\{1, R_{unc,t}\}$) on the approximated one, over the range of values shown in Figure 11. The values are reported in Table 6. By solving the model at second order, we are able to preserve the shape of the polynomial. Figure 11 shows that the approximation is valid in the range of quarterly interest rates between -4% and +4% (approximately -16% and +16% in annual figures).

Calibrated parameters

Table 7: Calibrated parameters. Note: The table reports the parameter's name (Full Name), the associate symbol (Symbol) and the calibrated value (Value).

Full Name	Symbol	Value
Labor share $\mathcal{S}_1$	α_1	0.350
Labor share $\mathcal{S}_2$	α_2	0.350
Discount factor	β	0.991
Depreciation $\mathcal{S}_1$	δ_{k_1}	0.025
Depreciation $\mathcal{S}_2$	δ_{k_2}	0.025
Mean of $a_{j,t}$	j^{ss}	0.072
Mean of $\phi_{1,t}$	ϕ_1^{ss}	0.643
Mean of $\phi_{2,t}$	ϕ_2^{ss}	1.896
Elast. final goods $\mathcal{S}_1$	ϵ_{π_1}	7.667
Elast. final goods $\mathcal{S}_2$	ϵ_{π_2}	7.667
Elast. labor $\mathcal{S}_1$	ϵ_{w_1}	7.667
Elast. labor $\mathcal{S}_2$	ϵ_{w_2}	7.667
Persistence Mon. Policy	ρ_s	0.975

References

Abo-Zaid, S. and Xuguang, S. S. (2020). Health Shocks in a General Equilibrium Model. Available at ssrn: https://ssrn.com/abstract=3611404.

Adjemian, S., Bastani, H., Juillard, M., Karamé, F., Mihoubi, F., Mutschler, W., Pfeifer, J., Ratto, M., Rion, N., and Villemot, S. (2022). Dynare: Reference Manual Version 5. Dynare Working Papers 72, CEPREMAP.

Alspach, D. and Sorenson, H. (1972). Nonlinear Bayesian Estimation Using Gaussian Sum Approximations. *IEEE transactions on automatic control*, 17:439–448.

Amisano, G. and Tristani, O. (2010). Euro Area Inflation Persistence in an Estimated Nonlinear DSGE model. *Journal of Economic Dynamics and Control*, 34:1837–1858.

Amisano, G. and Tristani, O. (2011). Exact Likelihood Computation for Nonlinear DSGE Models with Heteroskedastic Innovations. *Journal of Economic Dynamics and Control*, 35:2167–2185.

An, S. and Schorfheide, F. (2007). Bayesian Analysis of DSGE Models. *Econometric reviews*, 26:113–172.

Andreasen, M. M. (2011). Non-Linear DSGE Models and the Optimized Central Difference Particle Filter. *Journal of Economic Dynamics and Control*, 35:1671–1695.

Andreasen, M. M. (2012a). An Estimated DSGE Model: Explaining Variation in Nominal Term Premia, Real Term Premia, and Inflation Risk Premia. *European Economic Review*, 56:1656–1674.

Andreasen, M. M. (2012b). On the Effects of Rare Disasters and Uncertainty Shocks for Risk Premia in Non-Linear DSGE Models. *Review of Economic Dynamics*, 15:295–316.

Andreasen, M. M. (2013). Non-linear DSGE Models and the Central Difference Kalman Filter. *Journal of Applied Econometrics*, 28:929–955.

Arasaratnam, I. and Haykin, S. (2009). Cubature Kalman Filters. *IEEE Transactions on Automatic Control*, 54:1254–1269.

Arasaratnam, I., Haykin, S., and Elliott, R. J. (2007). Discrete-time Nonlinear Filtering Algorithms using Gauss–Hermite Quadrature. *Proceedings of the IEEE*, 95:953–977.

Aruoba, S. B., Cuba-Borda, P., Higa-Flores, K., Schorfheide, F., and Villalvazo, S. (2021). Piecewise-Linear Approximations and Filtering for DSGE Models with Occasionally Binding Constraints. *Review of Economic Dynamics*, 41:96–120.

Baqaee, D. R. and Farhi, E. (2021). Supply and Demand in Disaggregated Keynesian Economies with an Application to the Covid-19 Crisis. NBER Working Paper N. 27152.

Bengtsson, T., Bickel, P., Li, B., et al. (2008). Curse-of-Dimensionality Revisited: Collapse of the Particle Filter in Very Large Scale Systems. In *Probability and statistics: Essays in honor of David A. Freedman*, pages 316–334. Institute of Mathematical Statistics.

Benigno, G., Foerster, A., Otrok, C., and Rebucci, A. (2020). Estimating Macroeconomic Models of Financial Crises: An Endogenous Regime-Switching Approach. NBER Working Paper N. 26935.

Bernanke, B. S., Gertler, M., and Gilchrist, S. (1999). The Financial Accelerator in a Quantitative Business Cycle Framework. *Handbook of macroeconomics*, 1:1341–1393.

Binning, A. and Maih, J. (2015). Sigma Point Filters for Dynamic Nonlinear Regime Switching Models. Norges Bank Working Paper N. 10-2015.

Bodenstein, M., Corsetti, G., and Guerrieri, L. (2020). Social Distancing and Supply Disruptions in a Pandemic. CEPR Discussion Paper N. DP14629.

Brinca, P., Duarte, J. B., and Faria-e Castro, M. (2020). Measuring Sectoral Supply and Demand Shocks During COVID-19. Federal Reserve Board St.Louis Working paper 2020-011.

Cai, M., Del Negro, M., Herbst, E., Matlin, E., Sarfati, R., and Schorfheide, F. (2021). Online Estimation of DSGE Models. *The Econometrics Journal*, 24:33–58.

Cardani, R., Croitorov, O., Giovannini, M., Pfeiffer, P., Ratto, M., and Vogel, L. (2022). The Euro Area's Pandemic Recession: A DSGE-based Interpretation. *Journal of Economic Dynamics and Control*, 143:104512.

Carriero, A., Clark, T. E., Marcellino, M. G., and Mertens, E. (2022). Addressing COVID-19 Outliers in BVARs with Stochastic Volatility. *The Review of Economics and Statistics*, 11:1–38.

Chib, S. and Ramamurthy, S. (2014). DSGE Models with Student-t Errors. *Econometric Reviews*, 33:152–171.

Creal, D. D. (2007). Sequential Monte Carlo Samplers for Bayesian DSGE Models. *Manuscript, University Chicago Booth*, pages 245–296.

Creal, D. D. (2012). A Survey of Sequential Monte Carlo Methods for Economics and Finance. *Econometric reviews*, 31:245–296.

Creal, D. D. (2017). A Class of Non-Gaussian State Space Models With Exact Likelihood Inference. *Journal of Business & Economic Statistics*, 35:585–597.

Cúrdia, V., Del Negro, M., and Greenwald, D. L. (2014). Rare Shocks, Great Recessions. *Journal of Applied Econometrics*, 29:1031–1052.

Del Negro, M. and Schorfheide, F. (2008). Forming Priors for DSGE Models (and How it Affects the Assessment of Nominal Rigidities). *Journal of Monetary Economics*, 55:1191–1208.

del Rio-Chanona, R. M., Mealy, P., Pichler, A., Lafond, F., and Farmer, J. D. (2020). Supply and Demand Shocks in the COVID-19 Pandemic: An Industry and Occupation Perspective. *Oxford Review of Economic Policy*, 36:94–137.

Dewachter, H. and Wouters, R. (2014). Endogenous Risk in a DSGE Model with Capital-Constrained Financial Intermediaries. *Journal of Economic Dynamics and control*, 43:241–268.

Durbin, J. and Koopman, S. J. (2012). *Time Series Analysis by State Space Methods*. Oxford University Press.

Durham, G. and Geweke, J. (2014). Adaptive Sequential Posterior Simulators for Massively Parallel Computing Environments. In *Bayesian model comparison*. Emerald Group Publishing Limited.

Eichenbaum, M. S., Rebelo, S., and Trabandt, M. (2021). The Macroeconomics of Epidemics. *The Review of Financial Studies*, 34:5149–5187.

Eichenbaum, M. S., Rebelo, S., and Trabandt, M. (2022). Epidemics in the Neoclassical and New Keynesian Models. *Journal of Economic Dynamics and Controln*, 140:1–19.

Faria-e Castro, M. (2021). Fiscal Policy During a Pandemic. *Journal of Economic Dynamics & Control*, 125:104–135.

Faubel, F., McDonough, J., and Klakow, D. (2009). The Split and Merge Unscented Gaussian Mixture Filter. *IEEE Signal Processing Letters*, 16:786–789.

Fernández-Villaverde, J., Guerrón-Quintana, P., Rubio-Ramírez, J. F., and Uribe, M. (2011). Risk Matters: The Real Effects of Volatility Shocks. *American Economic Review*, 101:2530–2561.

Fernández-Villaverde, J. and Jones, C. I. (2022). Estimating and Simulating a SIRD Model of COVID-19 for Many Countries, States, and Cities. *Journal of Economic Dynamics and Control*, 140:104–130.

Fernández-Villaverde, J. and Rubio-Ramírez, J. F. (2007). Estimating Macroeconomic Models: A Likelihood Approach. *The Review of Economic Studies*, 74:1059–1087.

Ferroni, F., Fisher, J. D., and Melosi, L. (2022). Unusual Shocks in Our Usual Models. FRB of Chicago Working Paper No 2022-39.

Flury, T. and Shephard, N. (2011). Bayesian Inference Based Only on Simulated Likelihood: Particle Filter Analysis of Dynamic Economic Models. *Econometric Theory*, 27:933–956.

Fornaro, L. and Wolf, M. (2020). Covid-19 Coronavirus and Macroeconomic Policy. CEPR Discussion Paper N. DP14529.

Fornaro, L. and Wolf, M. (2023). The Scars of Supply Shocks: Implication for Monetary Policy. *Journal of Monetary Economics, Forthcoming.*

Gordon, N. J., Salmond, D. J., and Smith, A. F. (1993). Novel Approach to Nonlinear/Non-Gaussian Bayesian State Estimation. In *IEE proceedings F (radar and signal processing)*, volume 140, pages 107–113.

Gourio, F. (2012). Disaster Risk and Business Cycles. *American Economic Review*, 102:2734–2766.

Guerrieri, V., Lorenzoni, G., Straub, L., and Werning, I. (2020). Macroeconomic Implications of COVID-19: Can Negative Supply Shocks Cause Demand Shortages? NBER Working Paper N. 26918.

Herbst, E. and Schorfheide, F. (2014). Sequential Monte Carlo Sampling for DSGE Models. *Journal of Applied Econometrics*, 29:1073–1098.

Herbst, E. P. and Schorfheide, F. (2015). *Bayesian Estimation of DSGE Models*. Princeton University Press.

Iacoviello, M. and Neri, S. (2010). Housing Market Spillovers: Evidence from an Estimated DSGE Model. *American Economic Journal: Macroeconomics*, 2:125–164.

Ito, K. and Xiong, K. (2000). Gaussian Filters for Nonlinear Filtering Problems. *IEEE Transactions on Automatic Control*, 45:910–927.

Ivashchenko, S. (2014). DSGE Model Estimation on the Basis of Second-Order Approximation. *Computational Economics*, 43:71–82.

Jia, B., Xin, M., and Cheng, Y. (2013). High-Degree Cubature Kalman Filter. *Automatica*, 49:510–518.

Kaplan, G., Moll, B., and Violante, G. L. (2020). The Great Lockdown and the Big Stimulus: Tracing the Pandemic Possibility Frontier for the US. NBER Working Paper N. 27794.

Kollmann, R. (2015). Tractable Latent State Filtering for Non-linear DSGE Models Using a Second-Order Approximation and Pruning. *Computational Economics*, 45:239–260.

Kotecha, J. H. and Djuric, P. M. (2003). Gaussian-Sum Particle Filtering. *IEEE Transactions on Signal Processing*, 51:2602–2612.

Lenza, M. and Primiceri, G. E. (2022). How to Estimate a VAR after March 2020. *Journal of Applied Econometrics*, 37:688–699.

Leong, P. H., Arulampalam, S., Lamahewa, T. A., and Abhayapala, T. D. (2013). A Gaussian-Sum Based Cubature Kalman Filter for Bearings-Only Tracking. *IEEE Transactions on Aerospace and Electronic Systems*, 49:1161–1176.

Levintal, O. (2017). Fifth-Order Perturbation Solution to DSGE Models. *Journal of Economic Dynamics and Control*, 80:1–16.

Liu, J. S. and Chen, R. (1998). Sequential Monte Carlo Methods for Dynamic Systems. *Journal of the American Statistical Association*, 93:1032–1044.

Noh, S. (2020). Posterior Inference on Parameters in a Nonlinear DSGE Model via Gaussian-Based Filters. *Computational Economics*, 56:795–841.

Pei, H. L., Arulampalam, S., Lamahewa, A. T., and Abhayapala, D. T. (2013). A Gaussian-Sum Based Cubature Kalman Filter for Bearings-Only Tracking. *IEEE Transactions on Aerospace and Electronic Systems*, 49:1161–1176.

Pei, H. L., Arulampalam, S., Lamahewa, A. T., and Abhayapala, D. T. (2014). Gaussian-Sum Cubature Kalman Filter with Improved Robustness for Bearings-only Tracking. *IEEE Signal Processing Letters*, 21:513–517.

Pitt, M. K. and Shephard, N. (1999). Filtering Via Simulation: Auxiliary Particle Filters. *Journal of the American Statistical Association*, 94:590–599.

Primiceri, G. E. and Tambalotti, A. (2020). Macroeconomic Forecasting in the Time of COVID-19. *Manuscript, Northwestern University*, pages 1–23.

Richter, A. W. and Throckmorton, N. A. (2016). Is Rotemberg Pricing Justified by Macro Data? *Economics Letters*, 149:44–48.

Särkkä, S. (2013). *Bayesian Filtering and Smoothing*. Cambridge University Press.

Schmitt-Grohé, S. and Uribe, M. (2004). Solving Dynamic General Equilibrium Models Using a Second-Order Approximation to the Policy Function. *Journal of economic dynamics and control*, 28:755–775.

Smets, F. and Wouters, R. (2003). An Estimated Dynamic Stochastic General Equilibrium Model of the Euro Area. *Journal of the European Economic Association*, 1:1123–1175.

Smets, F. and Wouters, R. (2007). Shocks and Frictions in US Business Cycles: A Bayesian DSGE Approach. *American Economic Review*, 97:586–606.

Sorenson, H. W. and Alspach, D. L. (1971). Recursive Bayesian Estimation using Gaussian-Sums. *Automatica*, 7:465–479.

Wan, E. A. and Van Der Merwe, R. (2000). The Unscented Kalman Filter for Nonlinear Estimation. *Proceedings of the IEEE 2000 Adaptive Systems for Signal Processing, Communications, and Control Symposium*, 1:153–158.

Woodford, M. (2020). Effective Demand Failures and the Limits of Monetary Stabilization Policy. NBER Working Paper N. 27768.

RECENT PUBLICATIONS BY *CEIS Tor Vergata*

Three Liquid Assets
Nicola Amendola, Lorenzo Carbonari and Leo Ferraris
CEIS Research Paper, 516, October 2021

Efficient Nonparametric Estimation of Generalized Autocovariances
Alessandra Luati, Francesca Papagni and Tommaso Proietti
CEIS Research Paper, 515, October 2021

Partnership Dissolution with Cash-Constrained Agents
Guillaume Pommey
CEIS Research Paper, 514, October 2021

Pro-environmental Attitudes, Local Environmental Conditions and Recycling Behavior
Luisa Corrado, Andrea Fazio and Alessandra Pelloni
CEIS Research Paper, 513, September 2021

Pairs trading in the index options market
Marianna Brunetti and Roberta De Luca
CEIS Research Paper, 512, August 2021

Bribes, Lobbying and Industrial Structure
Roy Cerqueti, Raffaella Coppier and Gustavo Piga
CEIS Research Paper, 511, March 2021

Asset Pricing Using Block-Cholesky GARCH and Time-Varying Betas
Stefano Grassi and Francesco Violante
CEIS Research Paper, 510, March 2021

A News-based Policy Index for Italy: Expectations and Fiscal Policy
Daniela Fantozzi and Alessio Muscarnera
CEIS Research Paper, 509, March 2021

Seasonality in High Frequency Time Series
Tommaso Proietti and Diego J. Pedregal
CEIS Research Paper, 508, March 2021

Productivity, managers' social connections and the Great Recession
Iftekhar Hasan and Stefano Manfredonia
CEIS Research Paper, 507, March 2021

DISTRIBUTION

Our publications are available online at www.ceistorvergata.it

DISCLAIMER

The opinions expressed in these publications are the authors' alone and therefore do not necessarily reflect the opinions of the supporters, staff, or boards of CEIS Tor Vergata.

COPYRIGHT

MEDIA INQUIRIES AND INFORMATION

For media inquiries, please contact Barbara Piazzi at +39 06 72595652/01 or by e-mail at piazzi@ceis.uniroma2.it. Our web site, www.ceistorvergata.it, contains more information about Center's events, publications, and staff.

DEVELOPMENT AND SUPPORT

For information about contributing to CEIS Tor Vergata, please contact at +39 06 72595601 or by e-mail at segr.ceis@economia.uniroma2.it